Viscous Flow Simulations for Static Aeroelastic Analysis of a Wing at High-Lift Conditions

Advanced Modeling and Simulation Seminar Series

NASA Ames Research Center, October 15, 2015

Viscous Flow Simulations for Static Aeroelastic Analysis of a Wing at High-Lift Conditions

Advanced Modeling and Simulation Seminar Series

NASA Ames Research Center, October 15, 2015

H. Doğuş Akaydın, **Shayan Moini-Yekta** Science and Technology Corporation

Jeffrey Housman and **Nhan Nguyen** NASA Ames Research Center

in collaboration with **David Rodriguez** Science and Technology Corporation

and with support from **James Jensen** Arizona State University

Viscous Flow Simulations for Static Aeroelastic Analysis of a Wing at High-Lift Conditions

Advanced Modeling and Simulation Seminar Series

NASA Ames Research Center, October 15, 2015

Based on the paper AIAA 2015-2418 by Akaydın *et al.* presented at 33rd Applied Aerodynamics Conference in AIAA Aviation Forum in late July 2015.

Model Information

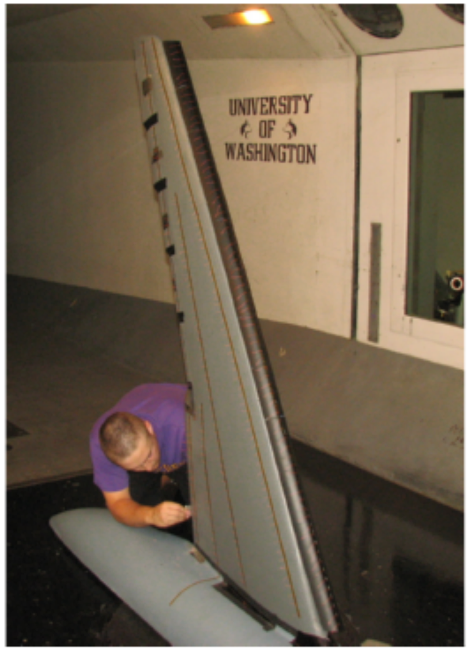

Wind tunnel tests were conducted at University of Washington Aeronautical Laboratory during the summer of 2014.

Bending and torsional stiffnesses of the wing is tailored to be representative of modern, composite-wing aircrafts.

Model Information

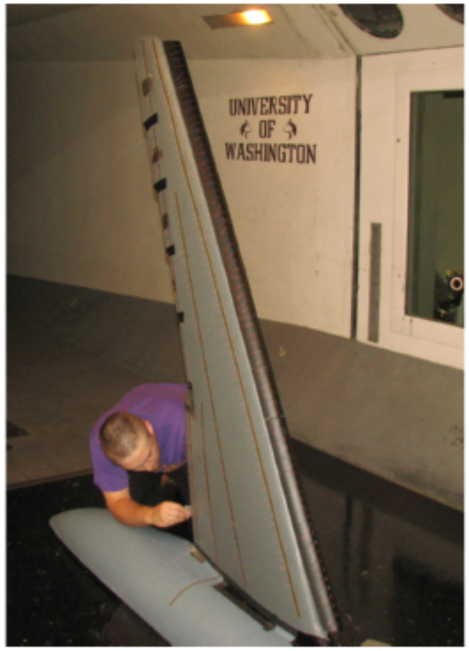

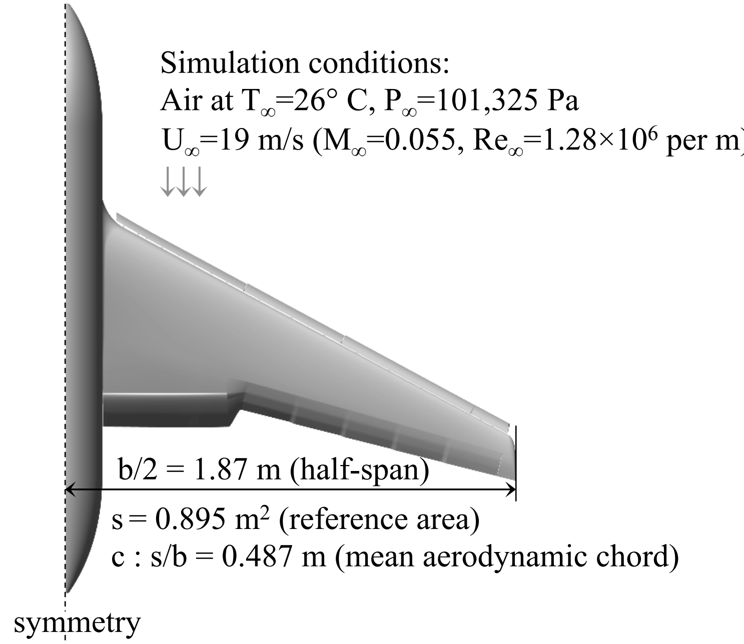

Model Information

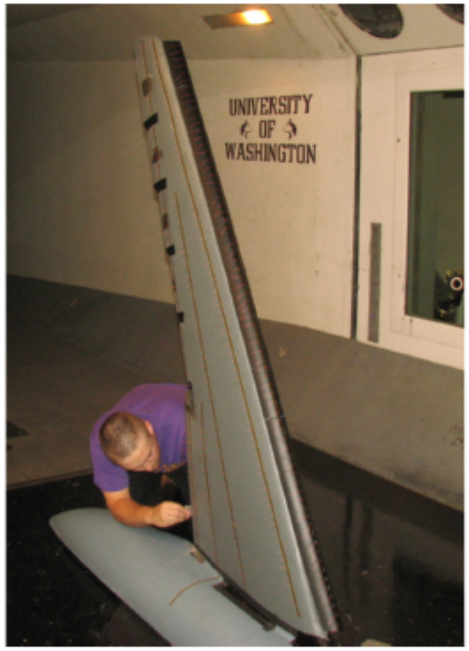

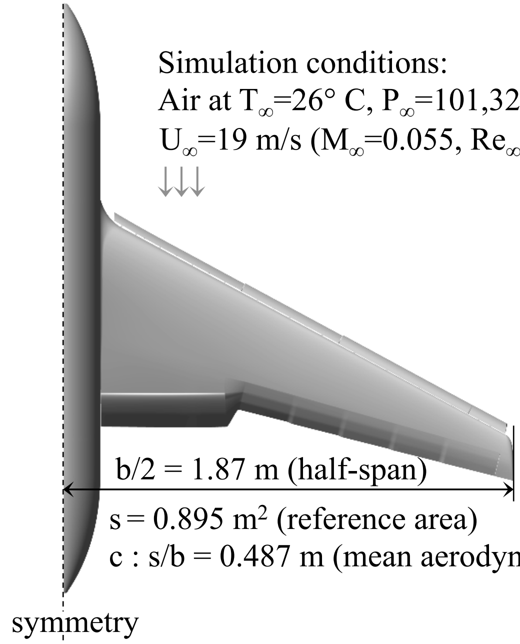

Simulation conditions:
Air at T_∞=26° C, P_∞=101,325 Pa
U_∞=19 m/s (M_∞=0.055, Re_∞=1.28×10^6 per m)

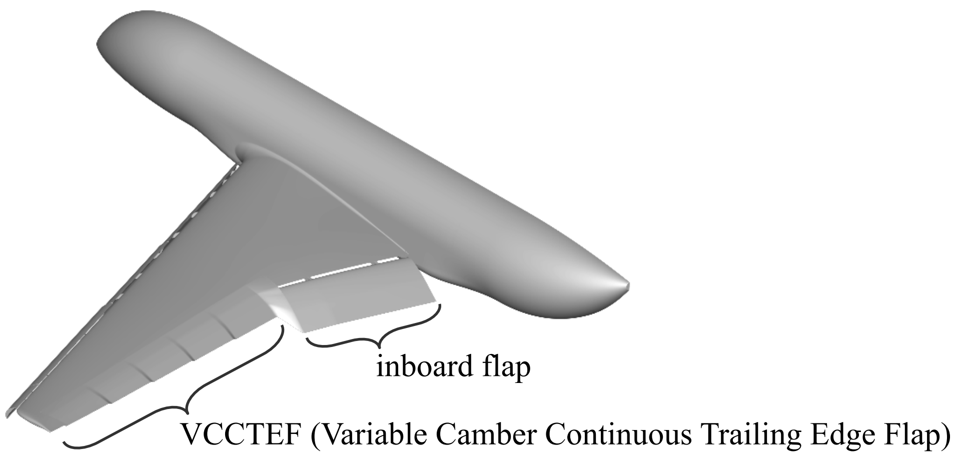

Model Information

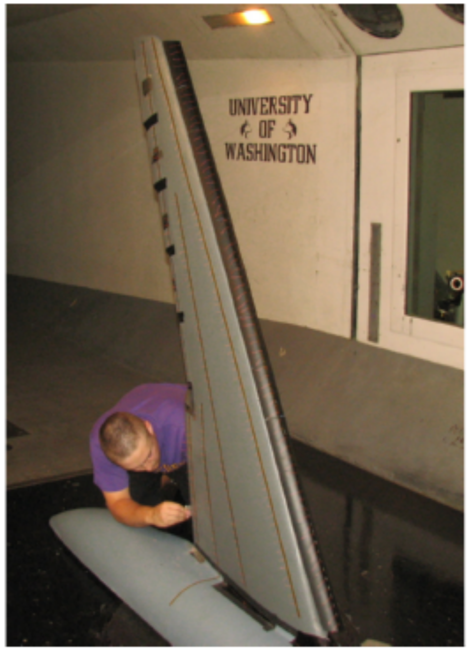

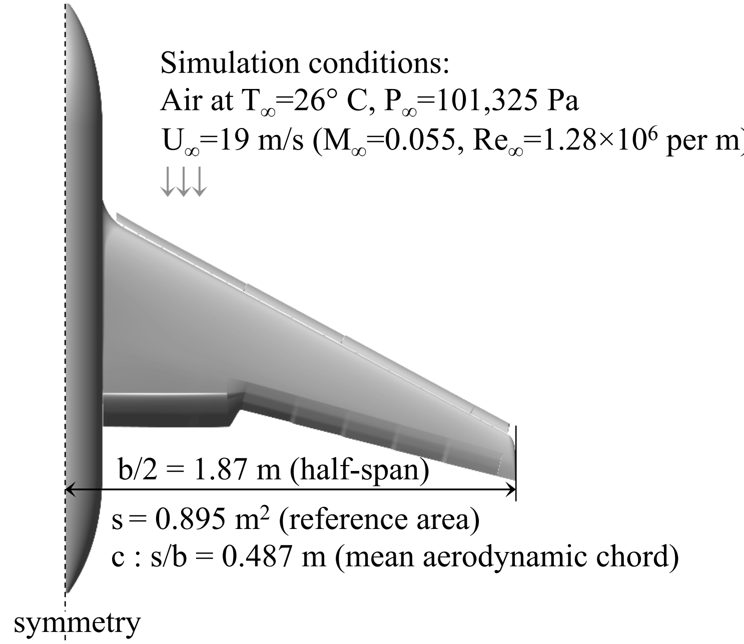

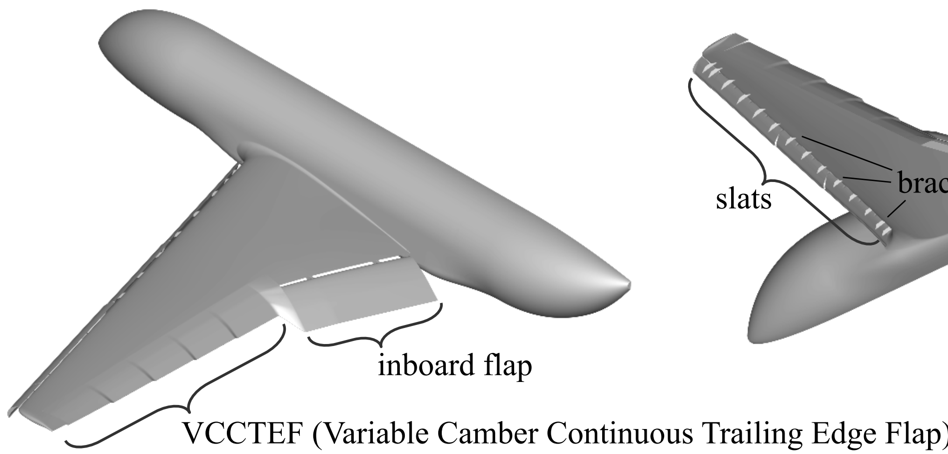

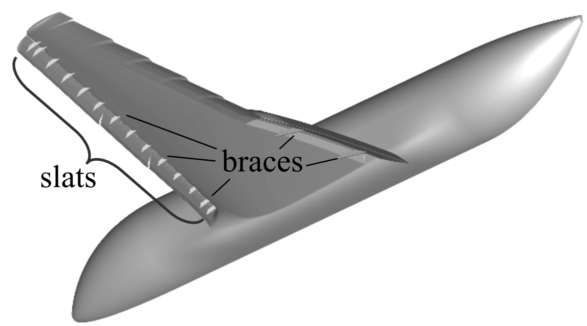

Grid System

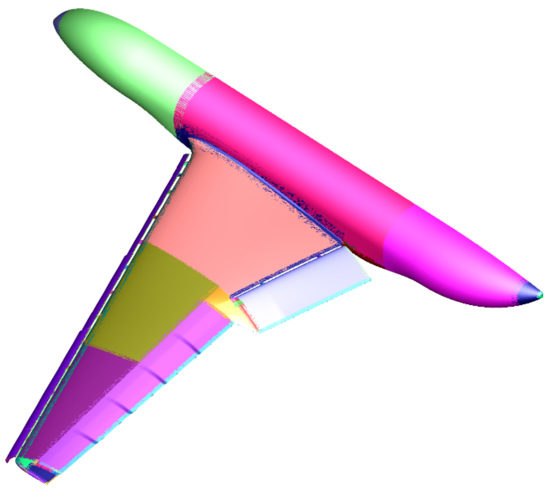

A structured, body-fitted overset grid system generated using CGT (Chimera Grid Tools) [1].

[1] Chan, W. *et al.* 2002 *Best Practices in Overset Grid Generation* 32nd AIAA Fluid Dynamics Conference and Exhibit, AIAA 2002-3191

Grid System

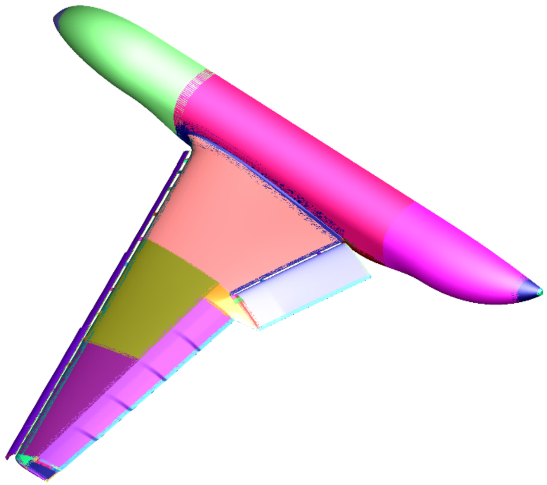

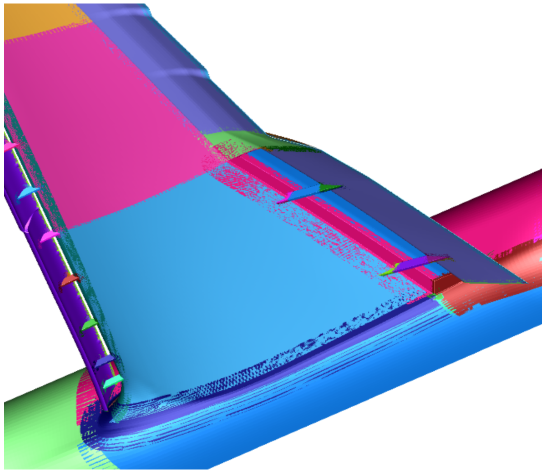

Grid System

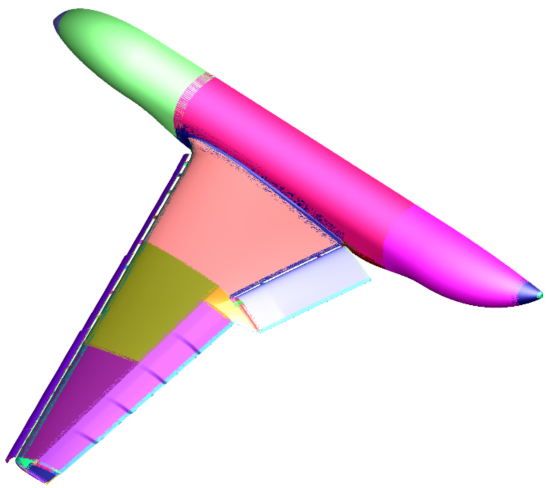

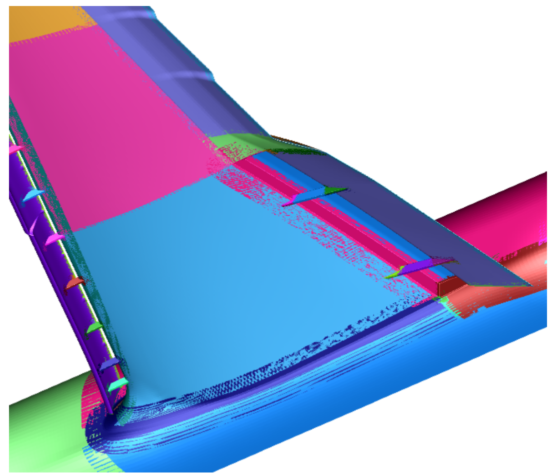

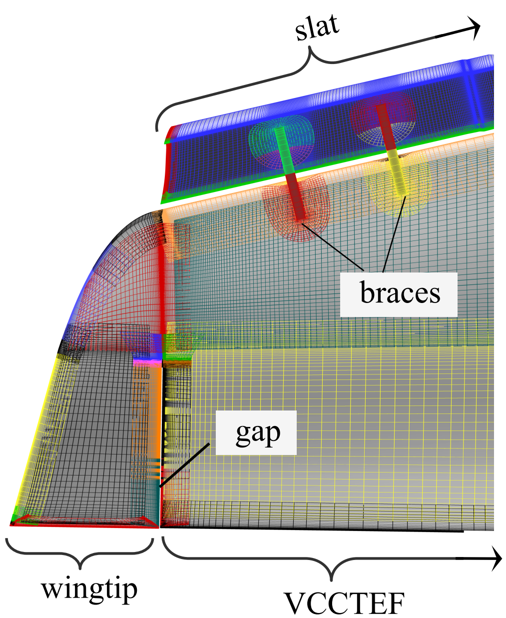
slat
braces
gap
wingtip
VCCTEF

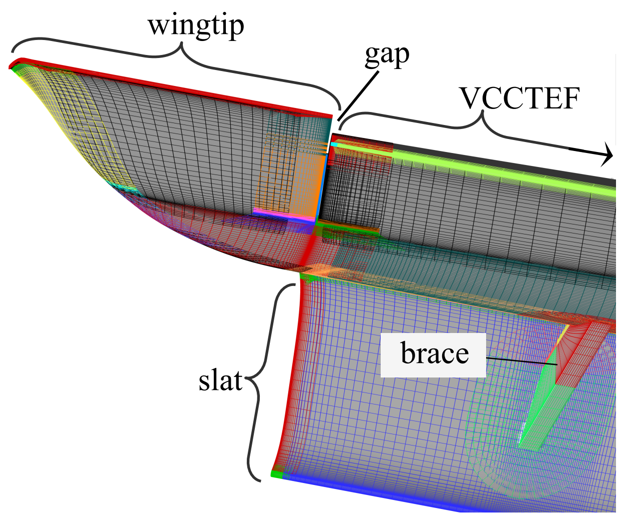
wingtip
gap
VCCTEF
slat
brace

Grid System

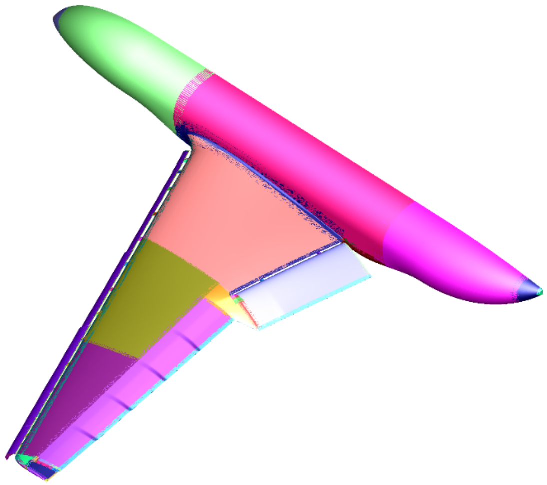

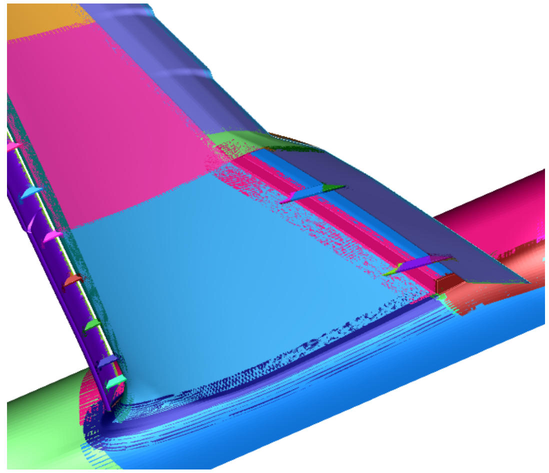

75 million vertices
4 off-body grid zones
that extend **30 body lengths** all around.
144 near-body grid zones with
$\mathbf{y^+ = 0.2}$ **to 0.3** on most surfaces

Overset connectivity is performed by DCF routine in Overflow 2.2g [2] using a donor quality factor of 0.5.

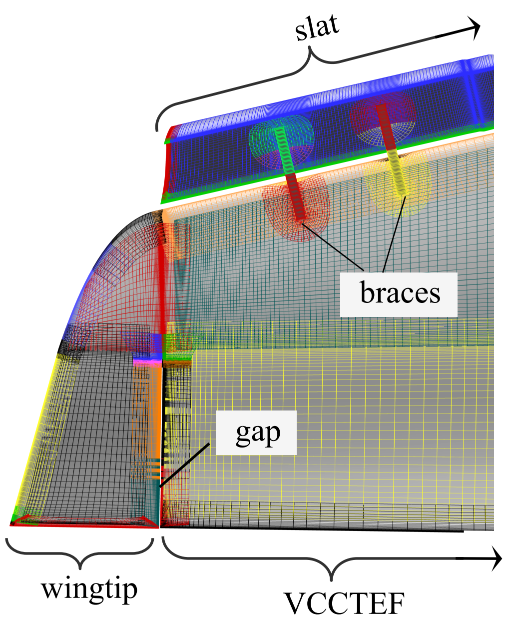

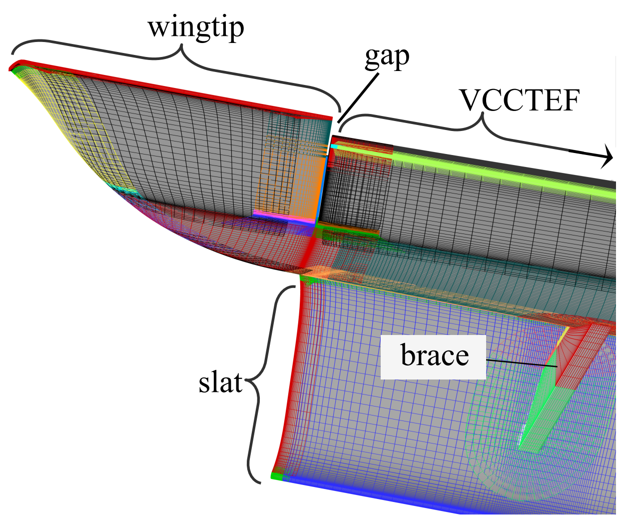

[2] Nichols, R. H. and Buning, P. G. 2010 *Users Manual for OVERFLOW 2.2* NASA Technical Report

Static Aeroelastic Analysis: Prior work with an inviscid solver

Rodriguez *et al*. [2] developed a static aeroelastic analysis framework by integrating an inviscid Euler flow solver (**Cart3D**), a structural analysis code (**BEAM**) and a geometry morphing tool (**Blender**):

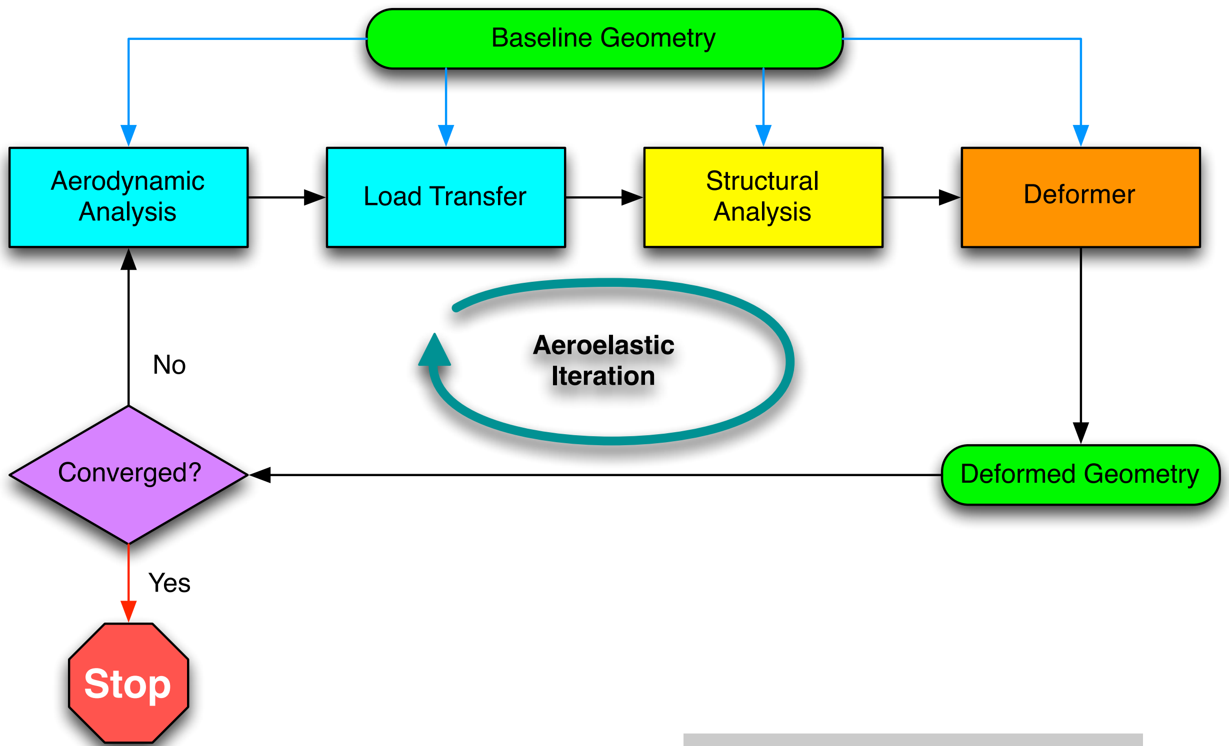

Courtesy of *Rodriguez, D. L.*

[2] Rodriguez, D. L. *et al*. 2014 *Static Aeroelastic Analysis with an Inviscid Cartesian Method* 55th Structures, Structural Dynamics and Materials Conference

[3] Aftosmis *et al*. 2000 *A Parallel Multilevel Method for Adaptively Refined Cartesian Grids with Embedded Boundaries* AIAA 2000-0808

Static Aeroelastic Analysis: Prior work with an inviscid solver

Flow field is solved by **Cart3D [3]**, a cartesian cut-cell finite volume code that solves Euler equations with adjoint-based adaptive mesh refinement.

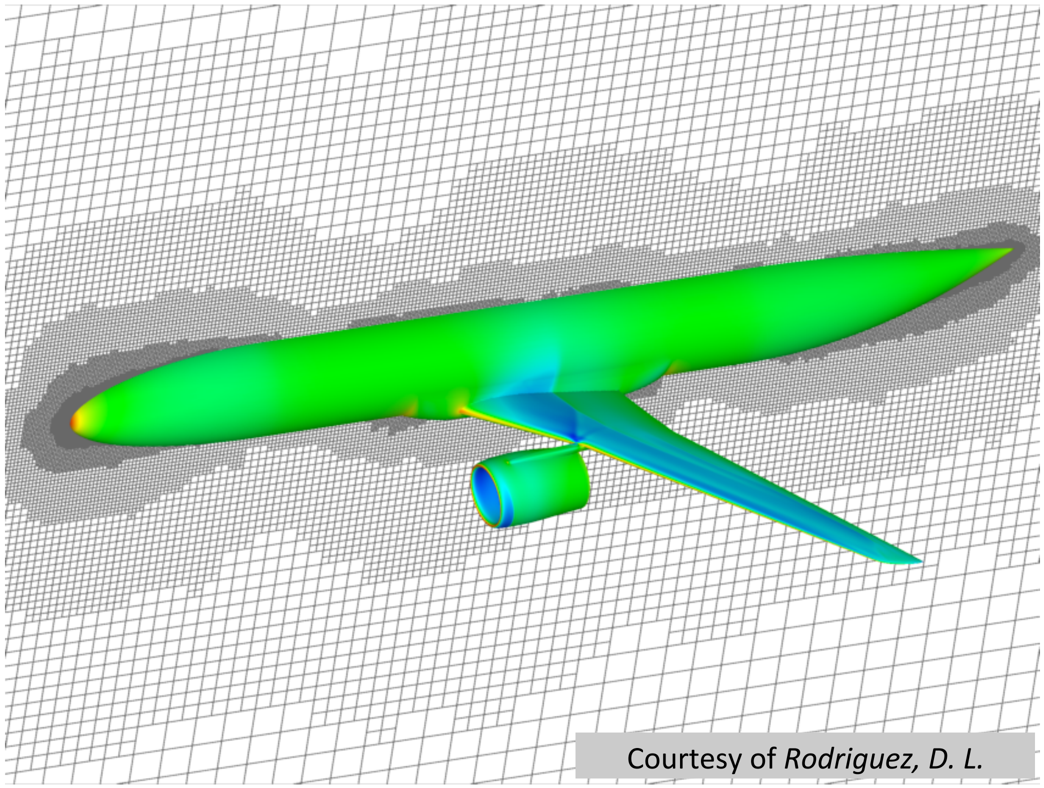

Courtesy of *Rodriguez, D. L.*

[3] Aftosmis *et al*. 2000 *A Parallel Multilevel Method for Adaptively Refined Cartesian Grids with Embedded Boundaries* AIAA 2000-0808

Static Aeroelastic Analysis: Prior work with an inviscid solver

Structural analysis is done by **BEAM**, a beam-element code that can model bending as well as torsion:

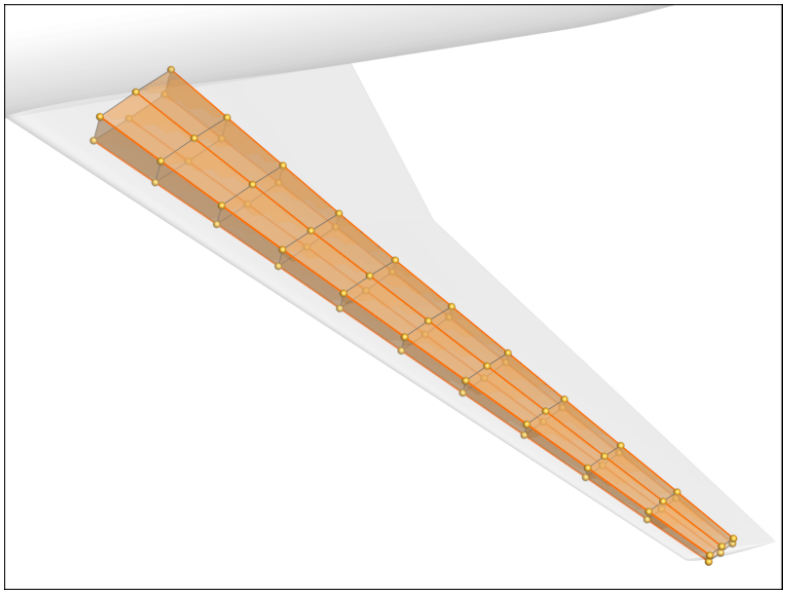

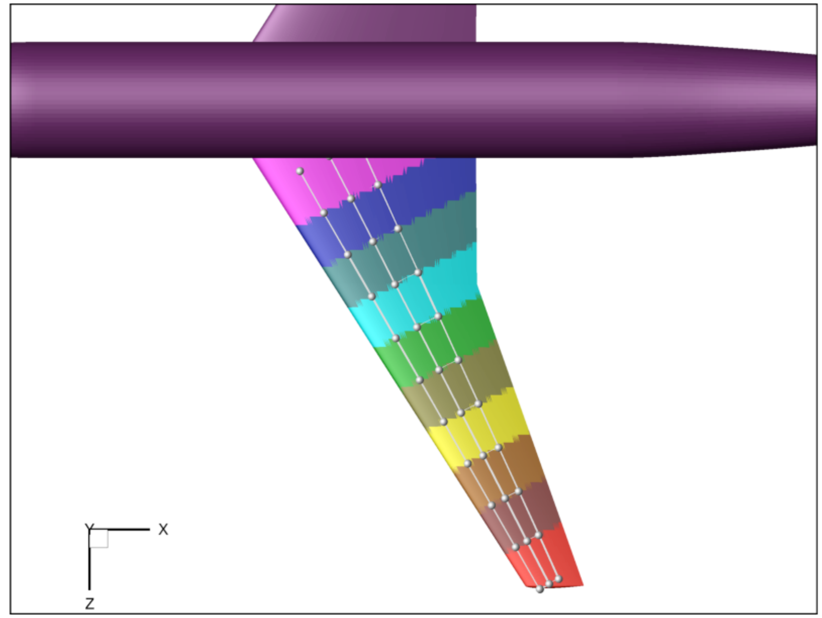

Courtesy of *Rodriguez, D. L.*

Bending stiffness (EI) and torsional stiffness (GJ) distributions are preset according to the experimental model.

[2] Rodriguez, D. L. *et al*. 2014 *Static Aeroelastic Analysis with an Inviscid Cartesian Method* 55th Structures, Structural Dynamics and Materials Conference

Static Aeroelastic Analysis: Prior work with an inviscid solver

Geometry deformation is done by **Blender**, an open-source geometry modeling and animation tool. It has a Python-based API and lattice deformer capability.

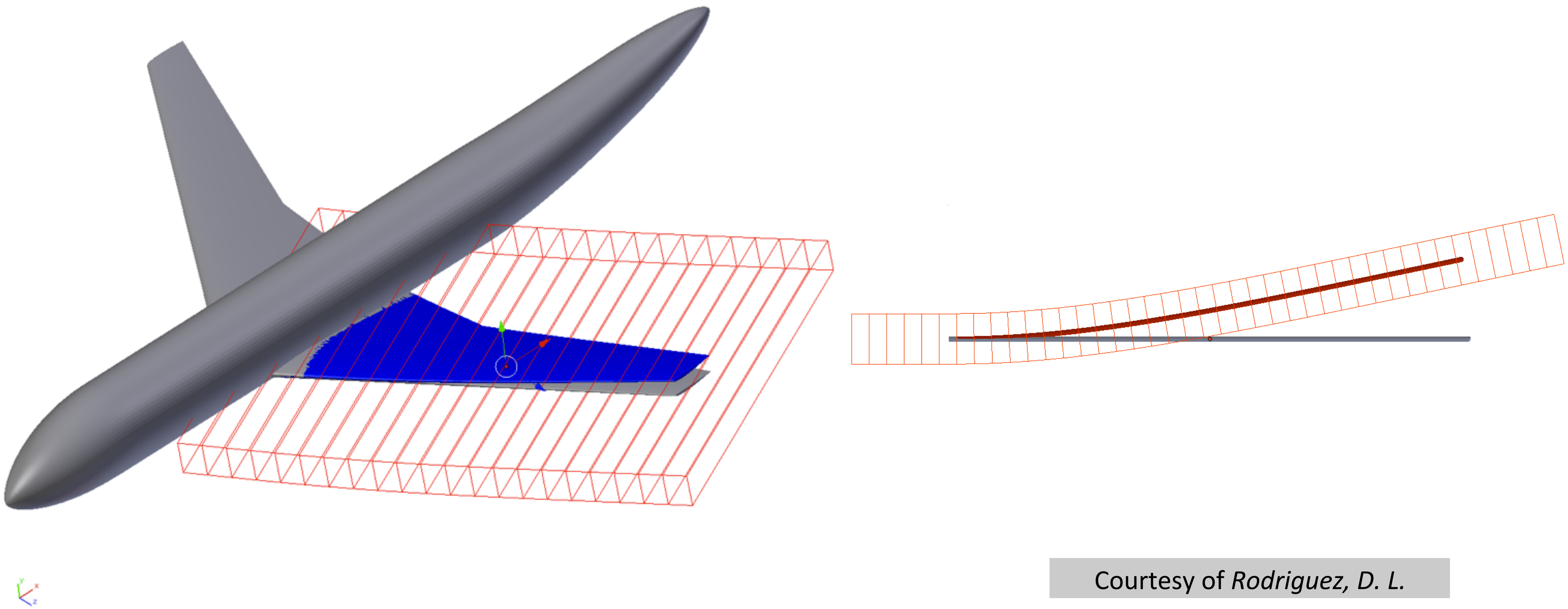

Courtesy of *Rodriguez, D. L.*

Viscous Flow Analysis

Viscous flow analysis is done by **Overflow** [3], an implicit, Reynolds-Averaged Navier-Stokes (RANS) solver developed by NASA for structured overset grids.

- Steady-state with constant CFL number
- Double fringe points
- Right-hand side: Roe's upwind scheme
- Left hand side: SSOR (Symmetric Successive Over-Relaxation)
- Low-Mach preconditioning enabled
- Turbulence model: Spalart-Allmaras (SA) model
- When setting up the input parameters, robustness was a priority over high accuracy.

[3] Nichols, R. H. and Buning, P. G. 2010 *Users Manual for OVERFLOW 2.2* NASA Technical Report

Static Aeroelastic Analysis: Viscous Solver Integration

Step 1: Generate non-deformed grids

- Generate a surface triangulation from CAD
- Generate a structured overset grid from that triangulation
- Generate a surface triangulation by splitting the structured surface grid cells in triangles
- Generate structured volume grids from structured surface grids, perform overset connectivity

For each angle of attack:

- Run S-S Overflow [3] simulations using the structured grid

Static Aeroelastic Analysis: Viscous Solver Integration

Step 1: Generate non-deformed grids

Step 2: Run inviscid aeroelastic analysis [2]
Around each angle of attack:
- Run S-S Cart3D on surface triangulation while targeting a suitable C_L [3]
- Using a beam element code deform (bend and twist) the wing of the CAD triangulation accordingly
- Iterate until converging to a final tip deflection
- Apply the same deformation on the structured grid triangulation and hole-cutter triangulations

Static Aeroelastic Analysis: Viscous Solver Integration

Step 1: Generate non-deformed grids

Step 2: Run inviscid aeroelastic framework

Step 3: Generate the deformed structured grid

For each deformed geometry in Step 2:

- Apply the nodal movements of the structured surface grid triangulation back onto the structured surface grid itself
- Regenerate volume grids based on the deformed surface grids, perform overset connectivity

Static Aeroelastic Analysis: Viscous Solver Integration

Step 1: Generate non-deformed grids

Step 2: Run inviscid aeroelastic framework

Step 3: Generate the deformed structured grid

For each deformed geometry in Step 2:

- Apply the nodal movements of the structured surface grid triangulation back onto the structured surface grid itself
- Regenerate volume grids based on the deformed surface grids, perform overset connectivity

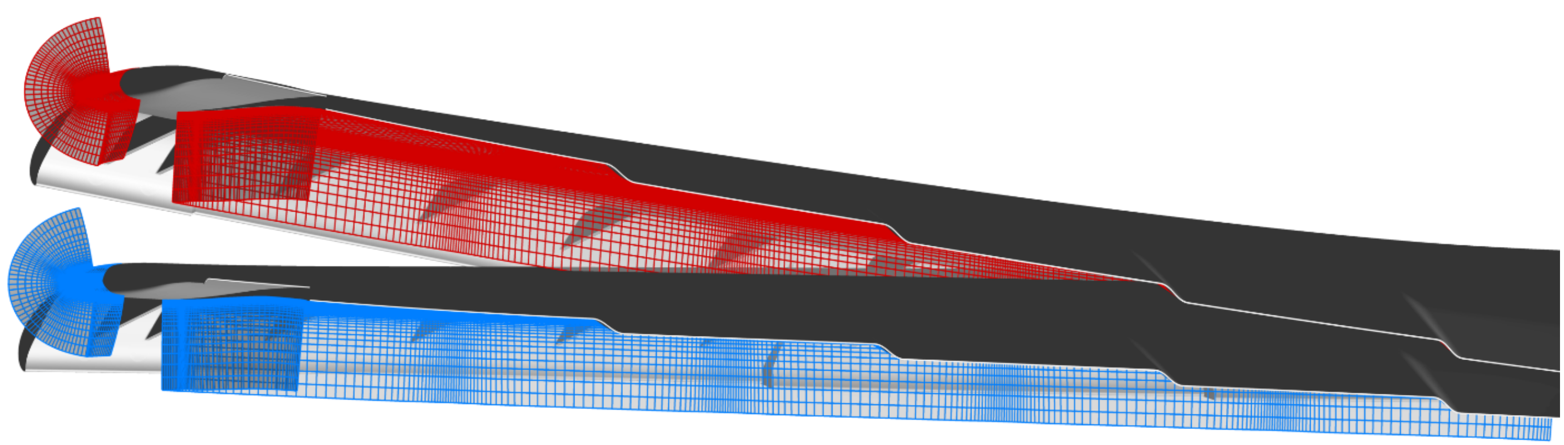

Static Aeroelastic Analysis: Viscous Solver Integration

Step 1: Generate non-deformed grids

Step 2: Run inviscid aeroelastic framework

Step 3: Generate the deformed structured grid

Step 4: Find viscous loads on deformed geometries

For each C_L targeted in Step 2:

- Run S-S Overflow simulations targeting that C_L while allowing angle of attack to change.

Static Aeroelastic Analysis: Viscous Solver Integration

Step 1: Generate non-deformed grids

Step 2: Run inviscid aeroelastic framework

Step 3: Generate the deformed structured grid

Step 4: Find viscous loads on deformed geometries

Step 5: Run additional Overflow simulations for a proper comparison

For each angle of attack found to in Step 4:

- Run S-S Overflow using the non-deformed geometry.

Static Aeroelastic Analysis: Viscous Solver Integration

Step 1: Generate non-deformed grids

Step 2: Run inviscid aeroelastic framework

Step 3: Generate the deformed structured grid

Step 4: Find viscous loads on deformed geometries

Step 5: Run additional Overflow simulations for a proper comparison

Cart3D simulations: 32 million cells in adapted grid. Converging for each angle of attack required around **4 steady-state solutions** that took about **6 hours** on **256 Sandy Bridge cores, each.** Time spent for beam elements analysis and deformation is negligible.

Static Aeroelastic Analysis: Viscous Solver Integration

Step 1: Generate non-deformed grids

Step 2: Run inviscid aeroelastic framework

Step 3: Generate the deformed structured grid

Step 4: Find viscous loads on deformed geometries

Step 5: Run additional Overflow simulations for a proper comparison

Overflow 2.2g simulations: Each simulation was ran in parallel on Pleiades Supercomputer at NASA Ames using **480 Sandy Bridge cores** and converged within **50 to 100 thousand flow iterations** (**20 to 40 hours** of wall time)

Static Aeroelastic Analysis: Viscous Solver Integration

Step 1: Generate non-deformed grids

Step 2: Run inviscid aeroelastic framework
~6 hours on 256 CPU cores per iter. (~4), per case (~10)
No labor for grid generation.

Step 3: Generate the deformed structured grid
~ a few minutes on a work station per case

Step 4: Find viscous loads on deformed geometries
Per each case
20 to 40 hours on 480 CPU cores per case
(>8 times more expensive than Cart3D)

Step 5: Run additional Overflow simulations for a proper comparison
20 to 40 hours on 480 CPU cores per case

Static Aeroelastic Analysis: Viscous Solver Integration

Step 1: Generate non-deformed grids
More than 1 person-month of labor for CAD preparation and grid generation!

Step 2: Run inviscid aeroelastic framework
~6 hours on 256 CPU cores per iter. (~4), per case (~10)
No labor for grid generation.

Step 3: Generate the deformed structured grid
~ a few minutes on a work station per case

Step 4: Find viscous loads on deformed geometries Per each case
20 to 40 hours on 480 CPU cores per case
(>8 times more expensive than Cart3D)

Step 5: Run additional Overflow simulations for a proper comparison
20 to 40 hours on 480 CPU cores per case

Results

Variation of total lift and drag with angle of attack:

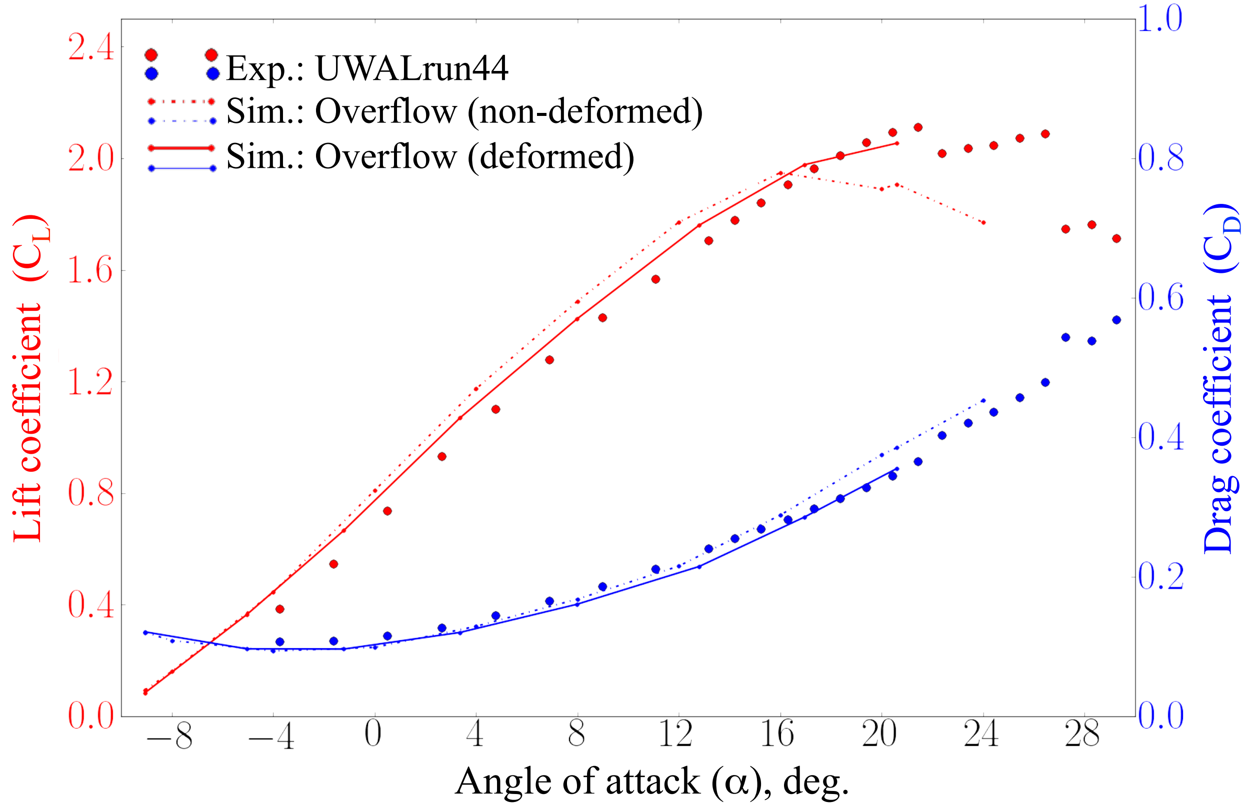

Results

Variation of total lift and drag with angle of attack:

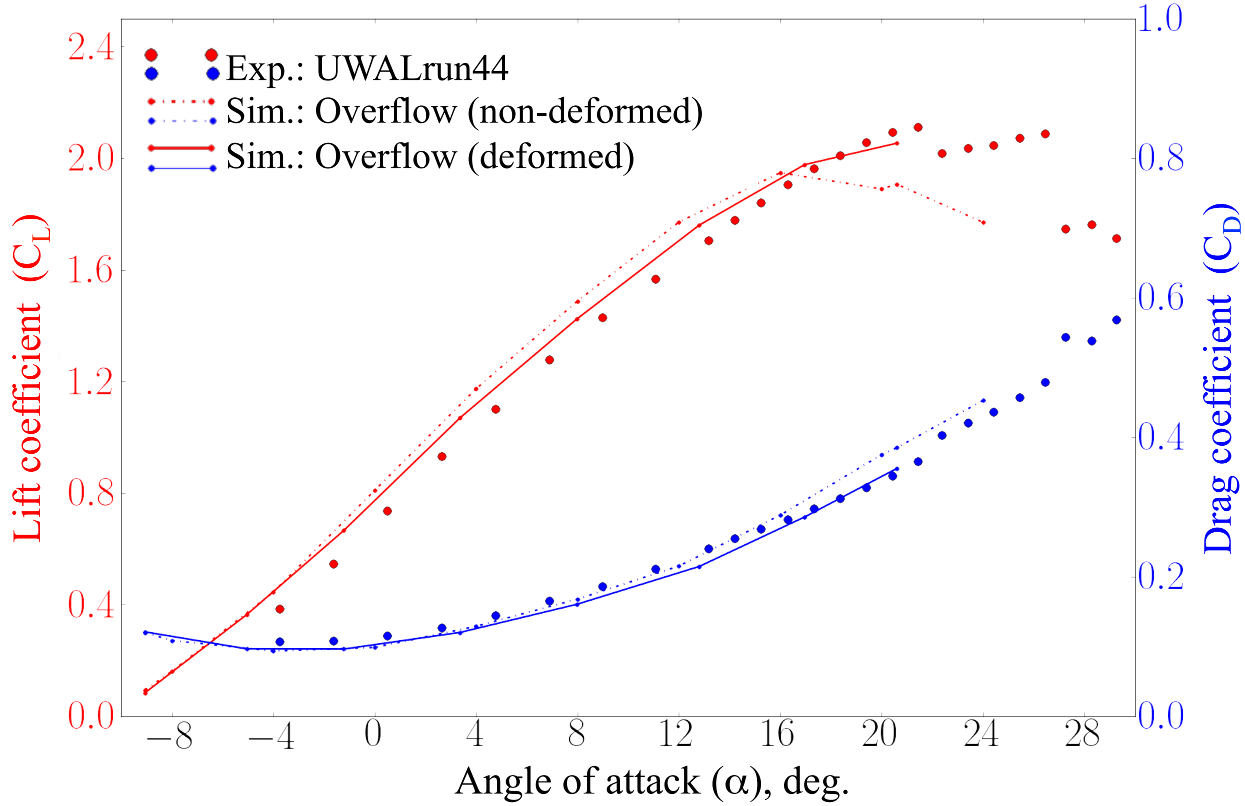

Observations:

- Deformation brings the lift prediction closer to the experimental results.

Results

Variation of total lift and drag with angle of attack:

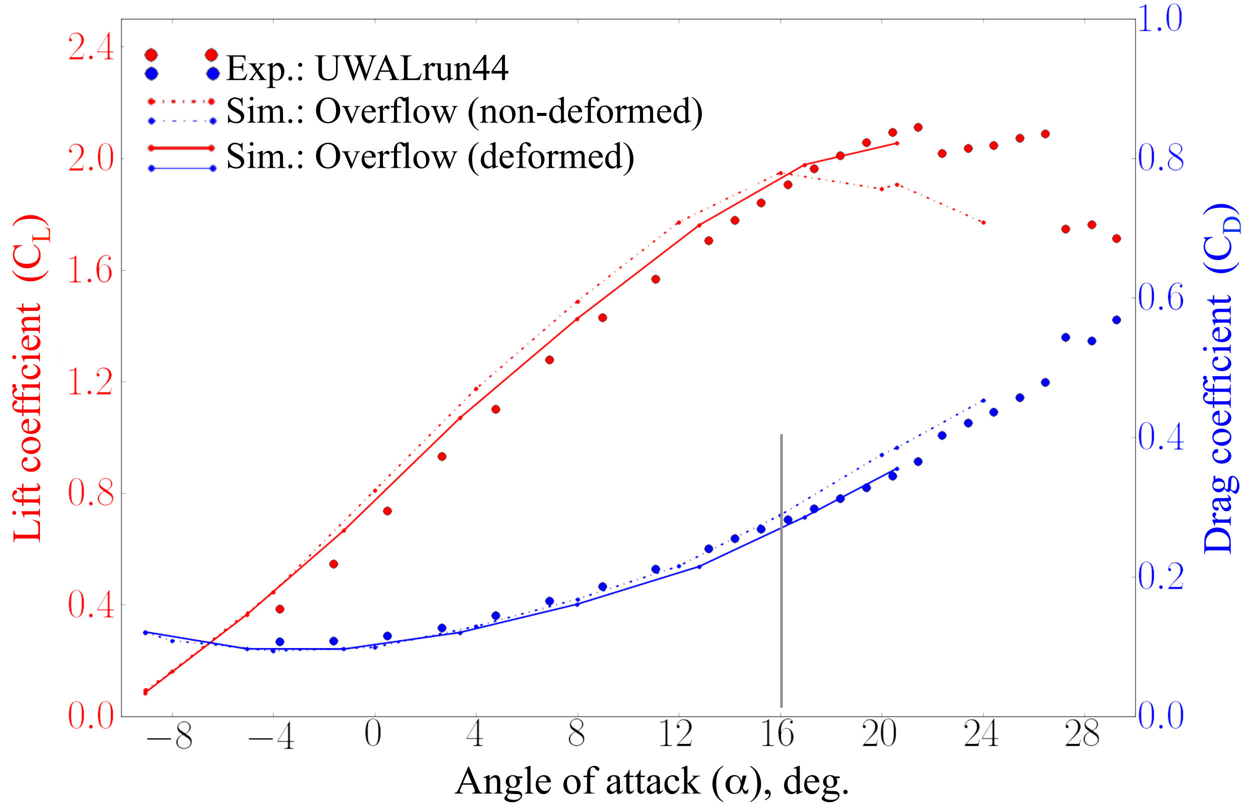

Observations:

- Deformation brings the lift prediction closer to the experimental results.
- **Drag prediction with the deformed geometry is reasonably good, especially when α>16°.**

Results

Variation of total lift and drag with angle of attack:

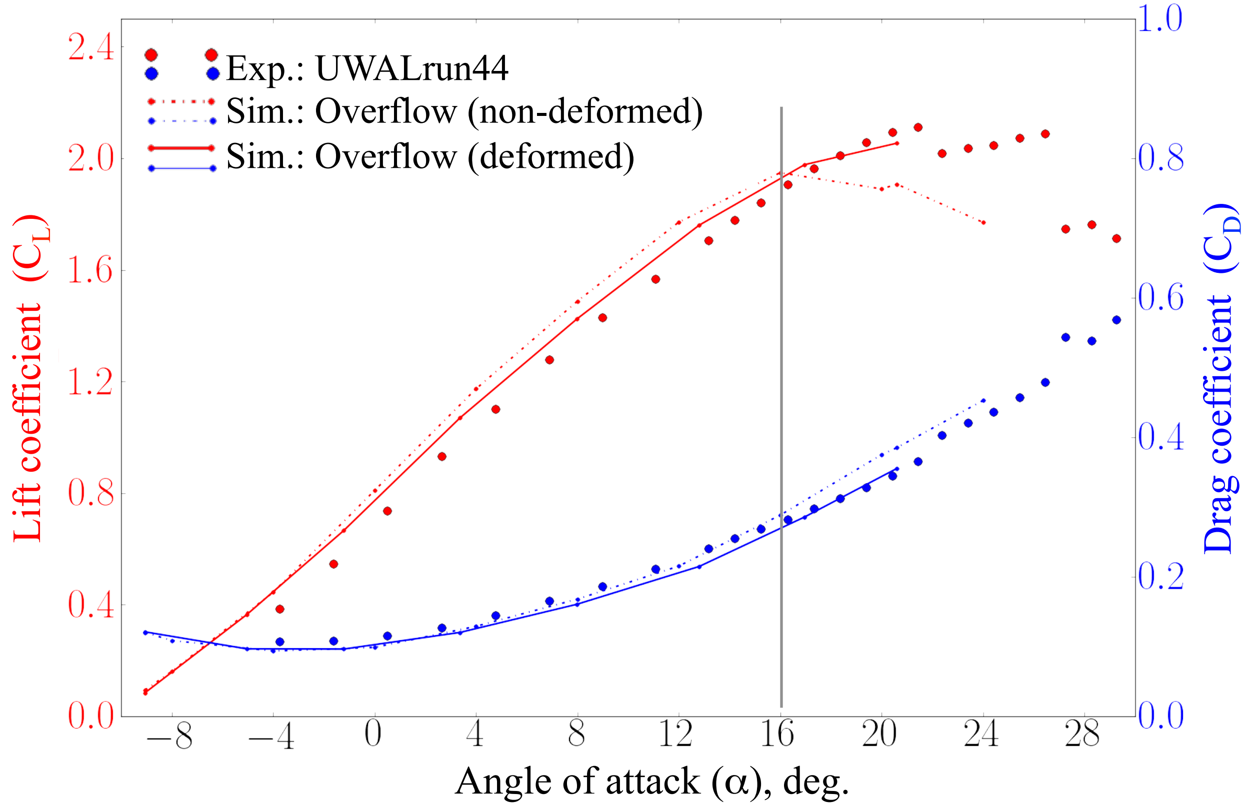

Observations:

- Deformation brings the lift prediction closer to the experimental results.
- Drag prediction with the deformed geometry is reasonably good, especially when α>16°.
- **Deformed geometry has a less total lift than non-deformed one when α<16°.**
- **Deformed geometry has a more total lift than non-deformed one when α>16°.**

Results

Variation of total lift and drag with angle of attack:

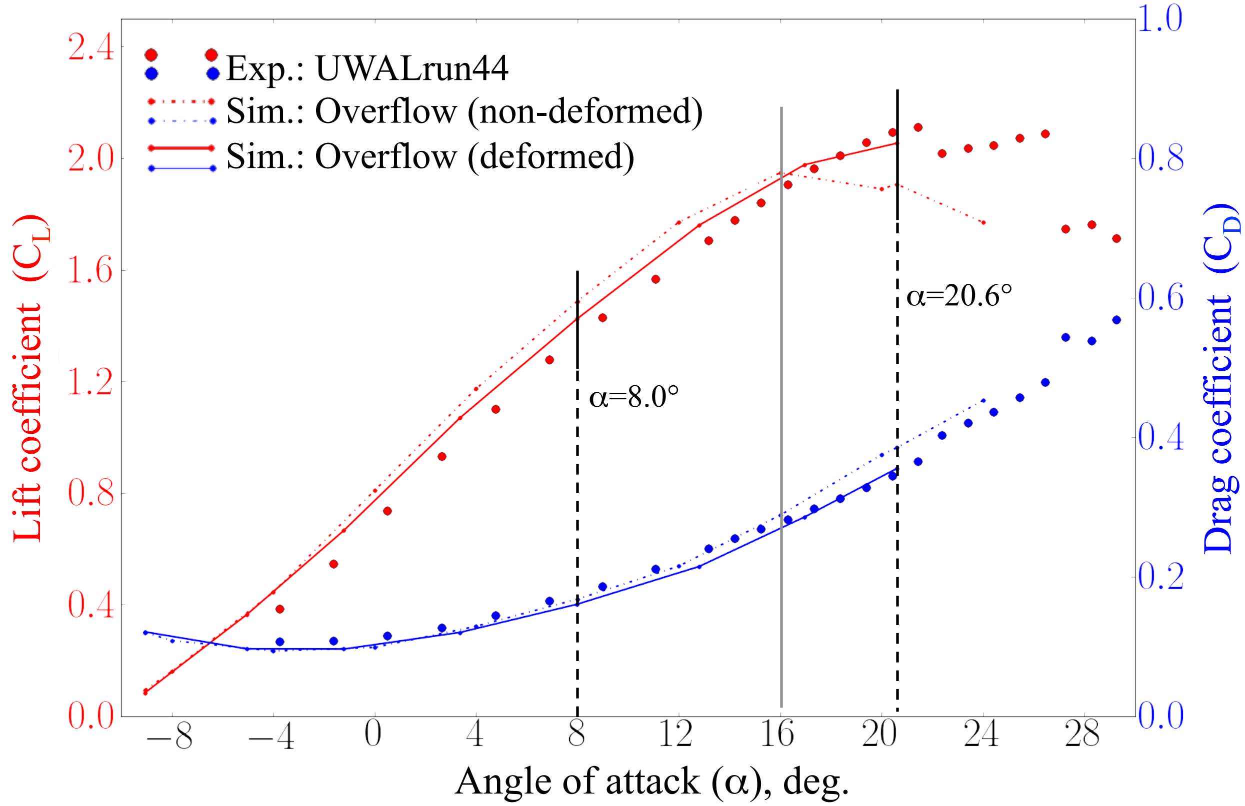

Observations:

- Deformation brings the lift prediction closer to the experimental results.
- Drag prediction with the deformed geometry is reasonably good, especially when α>16°.
- Deformed geometry has a less total lift than non-deformed one when α<16°.
- Deformed geometry has a more total lift than non-deformed one when α>16°.

Pick α=8.0° and α=20.6° for further analysis.

Detailed Analysis

Variation of surface pressure coefficients and streamlines at α=8.0°

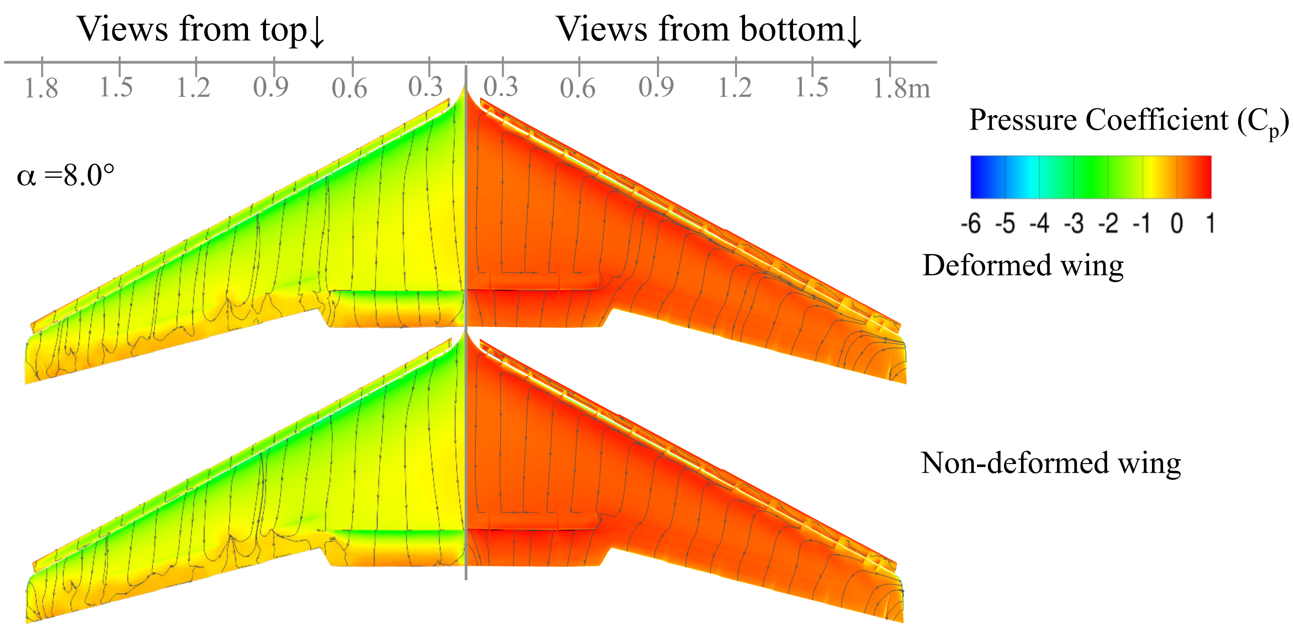

Detailed Analysis

Variation of surface pressure coefficients and streamlines at α=8.0°

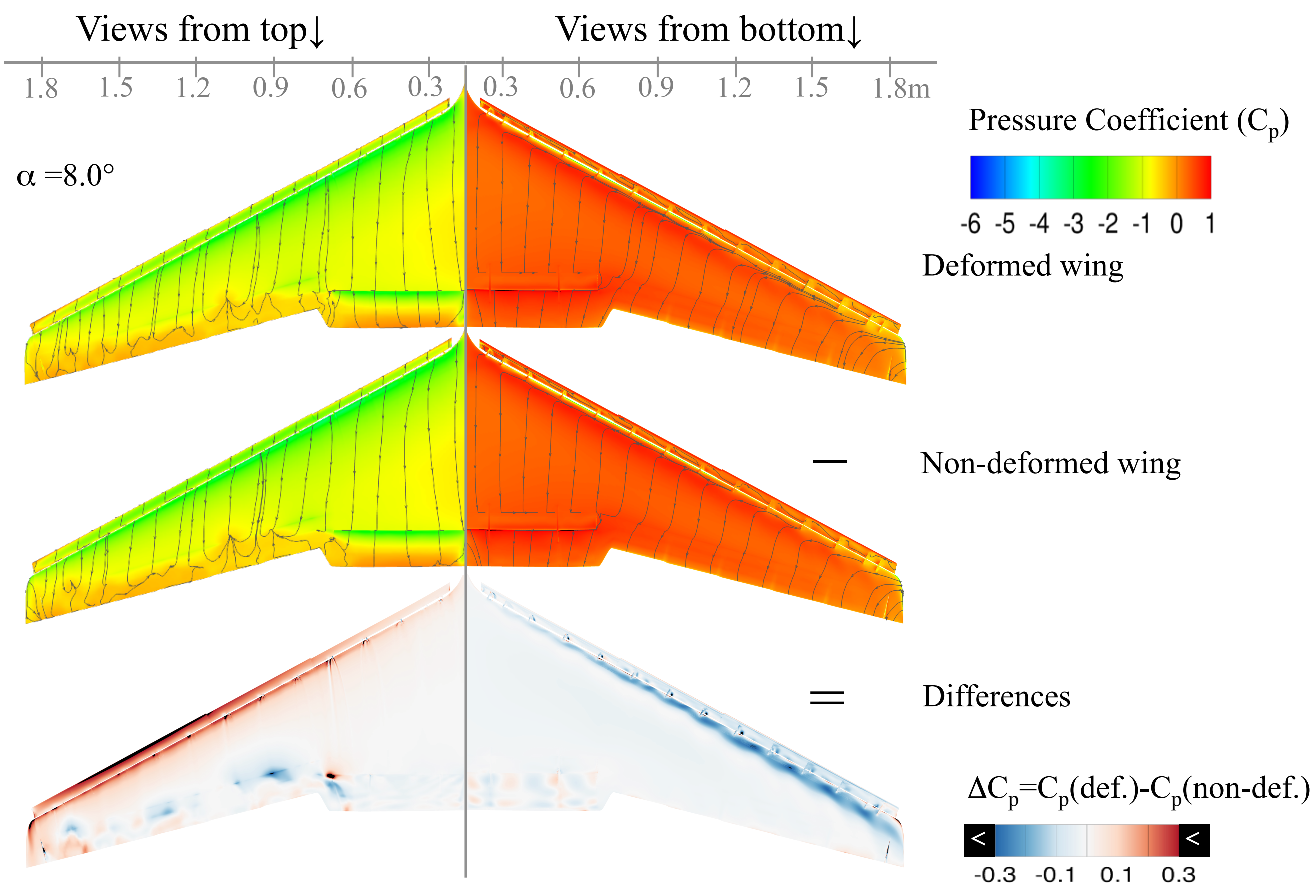

Detailed Analysis

Variation of surface pressure coefficients and streamlines at α=8.0°

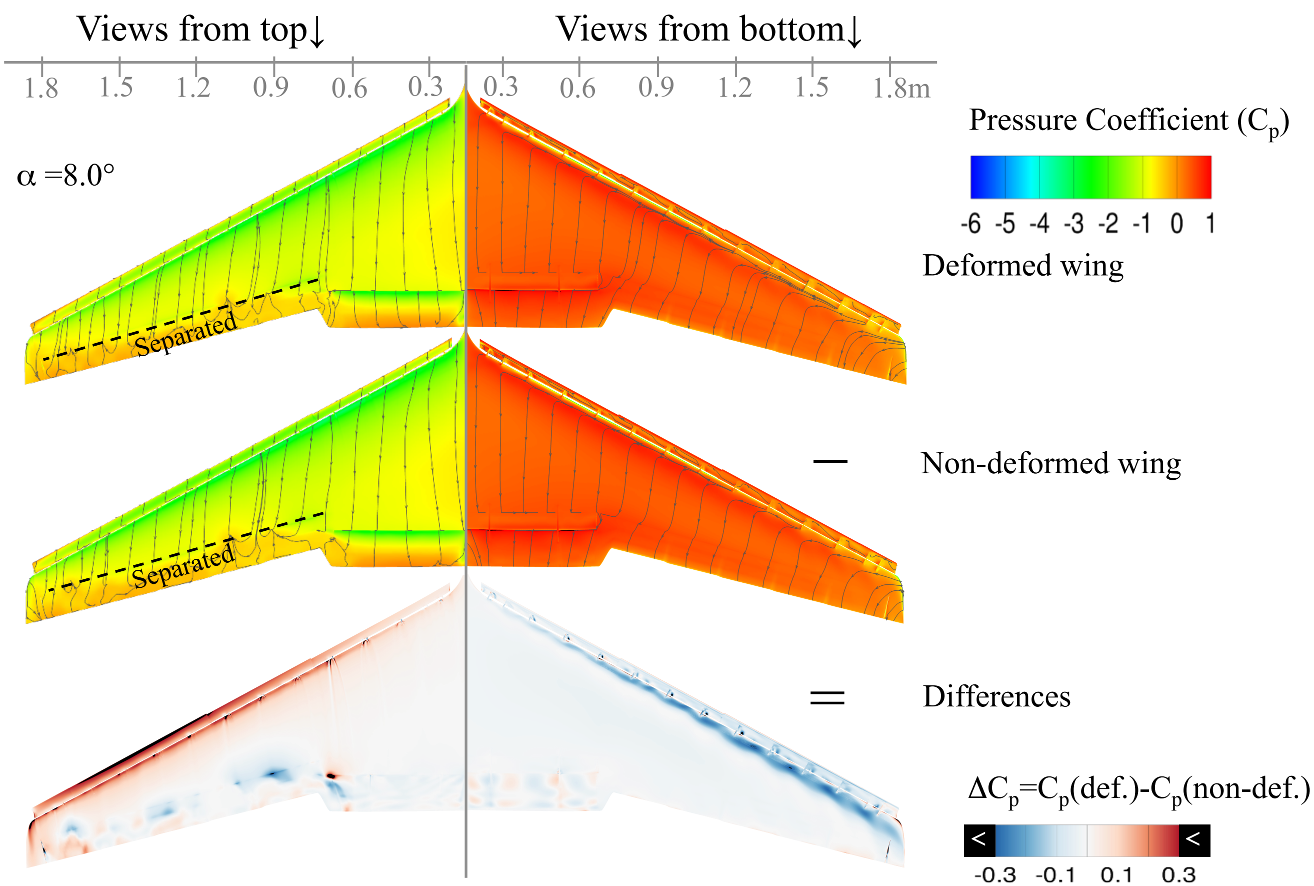

- Separation is small and wing deformation does not seem to increase it.
- Deformation decreases suction on top and pressure on bottom surfaces.
- Differences in C_p due to deformation on both surfaces are mild, and they seem to be changing gradually along the leading edge.
- Separation does not play a major role in lift decrease.

Detailed Analysis

Variation of surface pressure coefficients and streamlines at α=20.6°

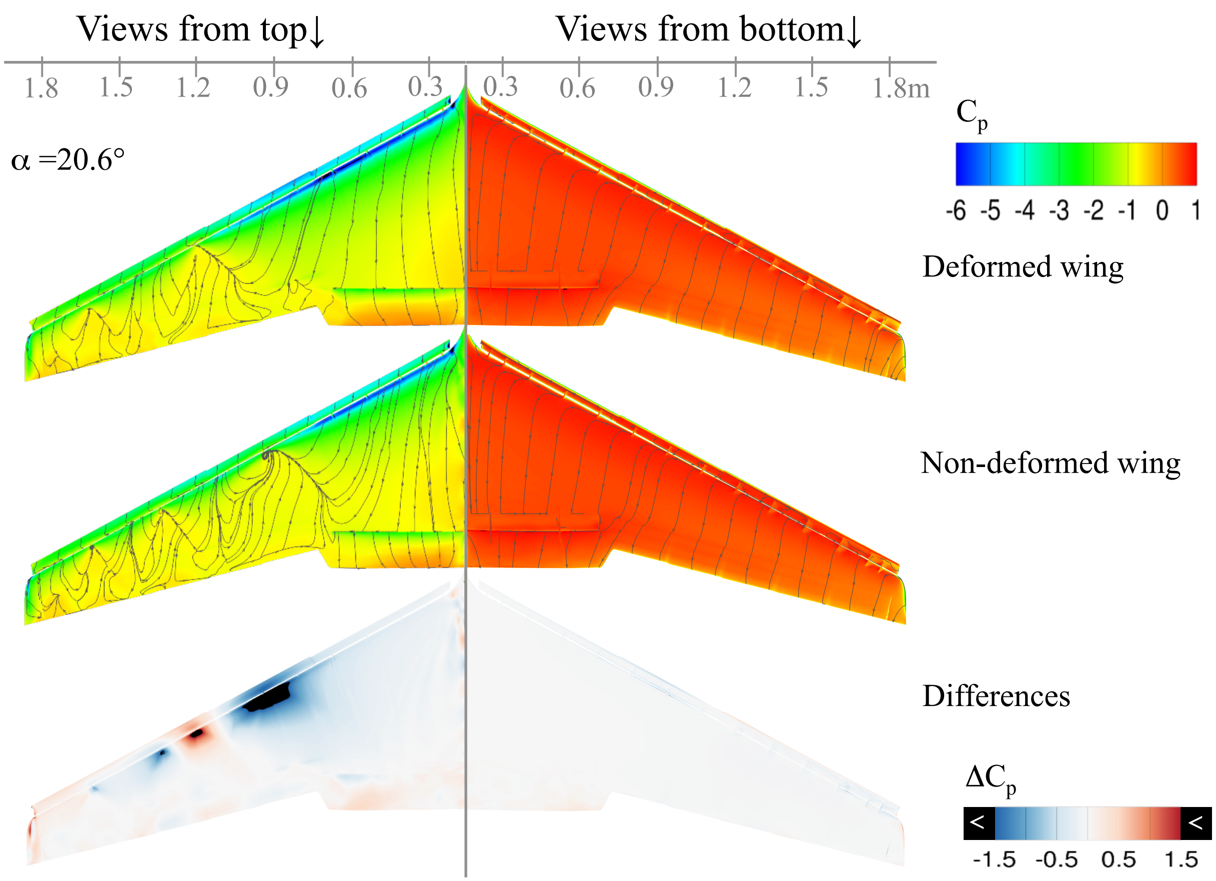

Detailed Analysis

Variation of surface pressure coefficients and streamlines at α=20.6°

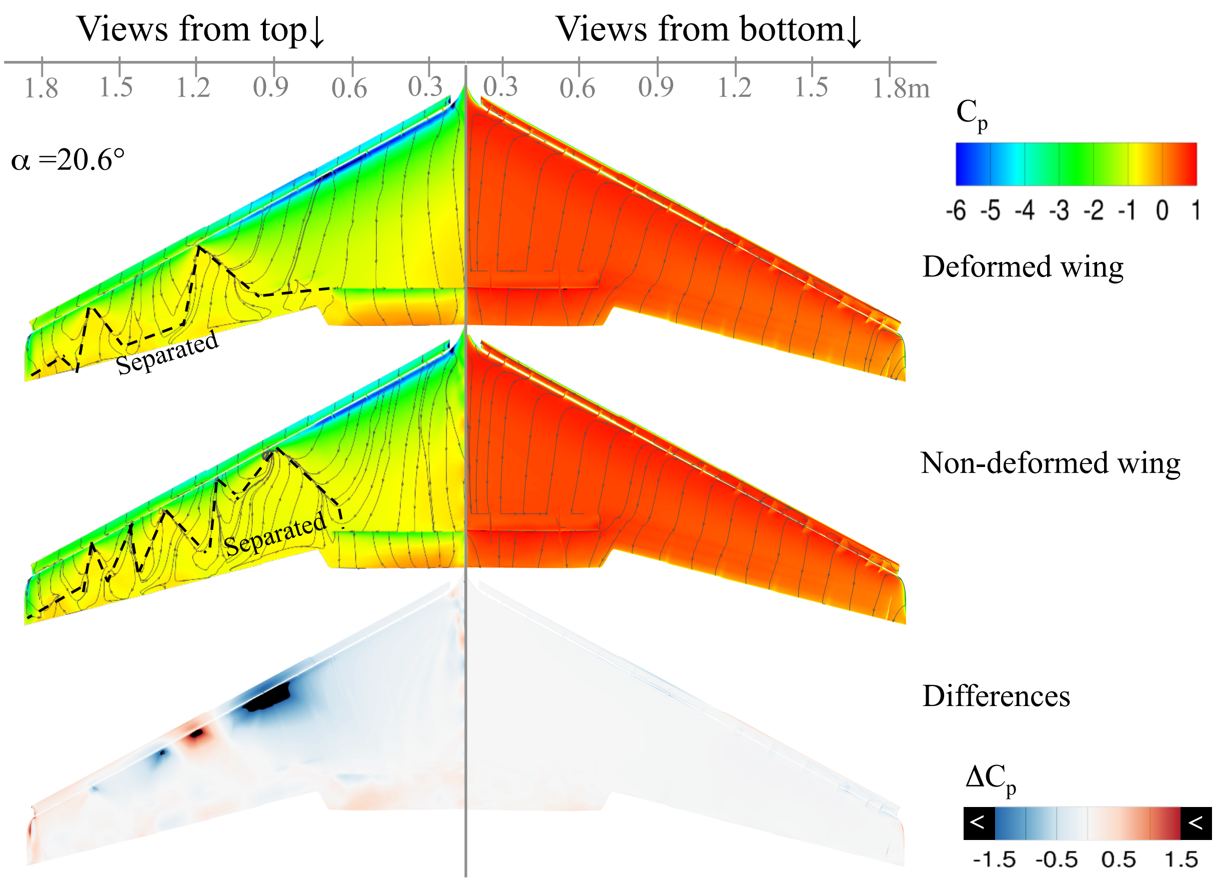

- On deformed wing, separation is large - covers a large outboard area beyond y = 1.1m
- On non-deformed wing, separation is even larger (covers most of the area beyond y=0.7m)
- Separation patterns seem to stem from the braces that connect slat to the main element.
- Differences in C_p is relatively large; and they have an alternating pattern reminiscent of the separation patterns.

Detailed Analysis

Sectional variations:

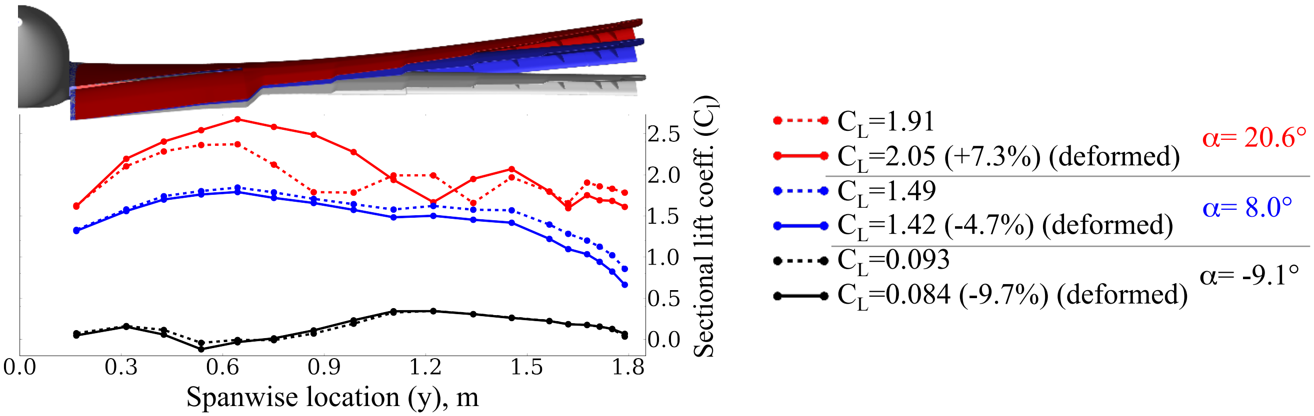

Detailed Analysis

Sectional variations:

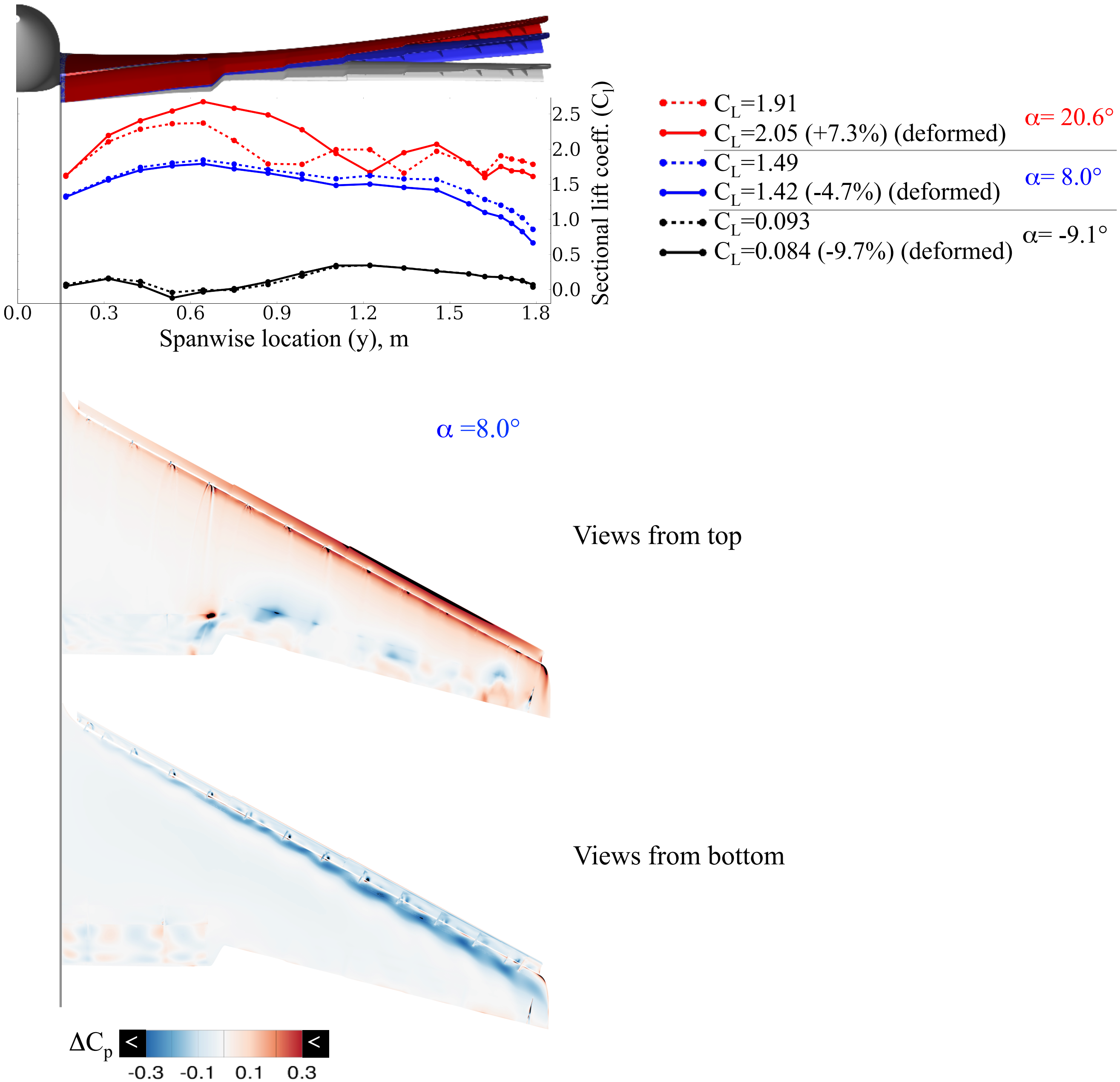

Detailed Analysis

Sectional variations:

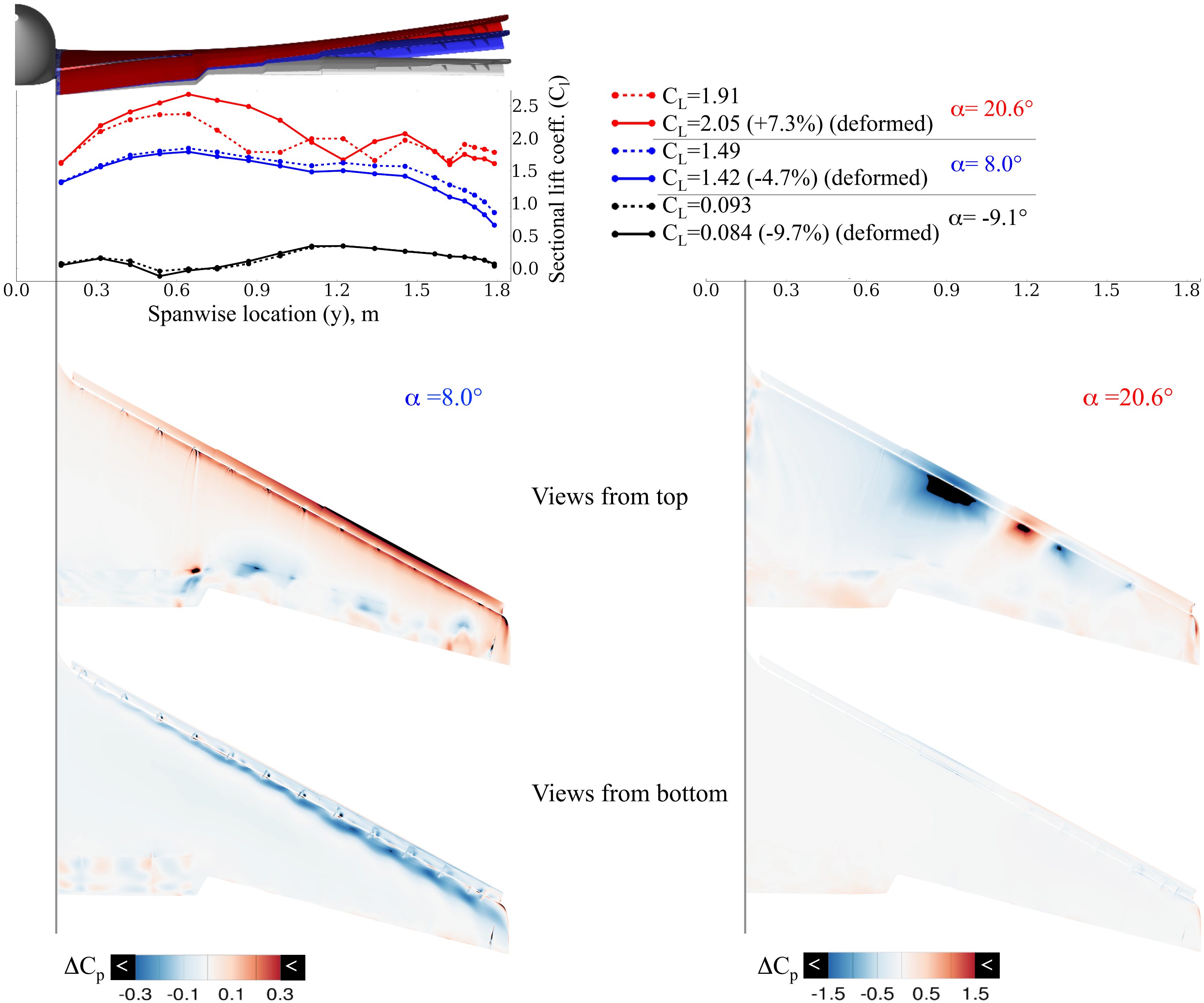

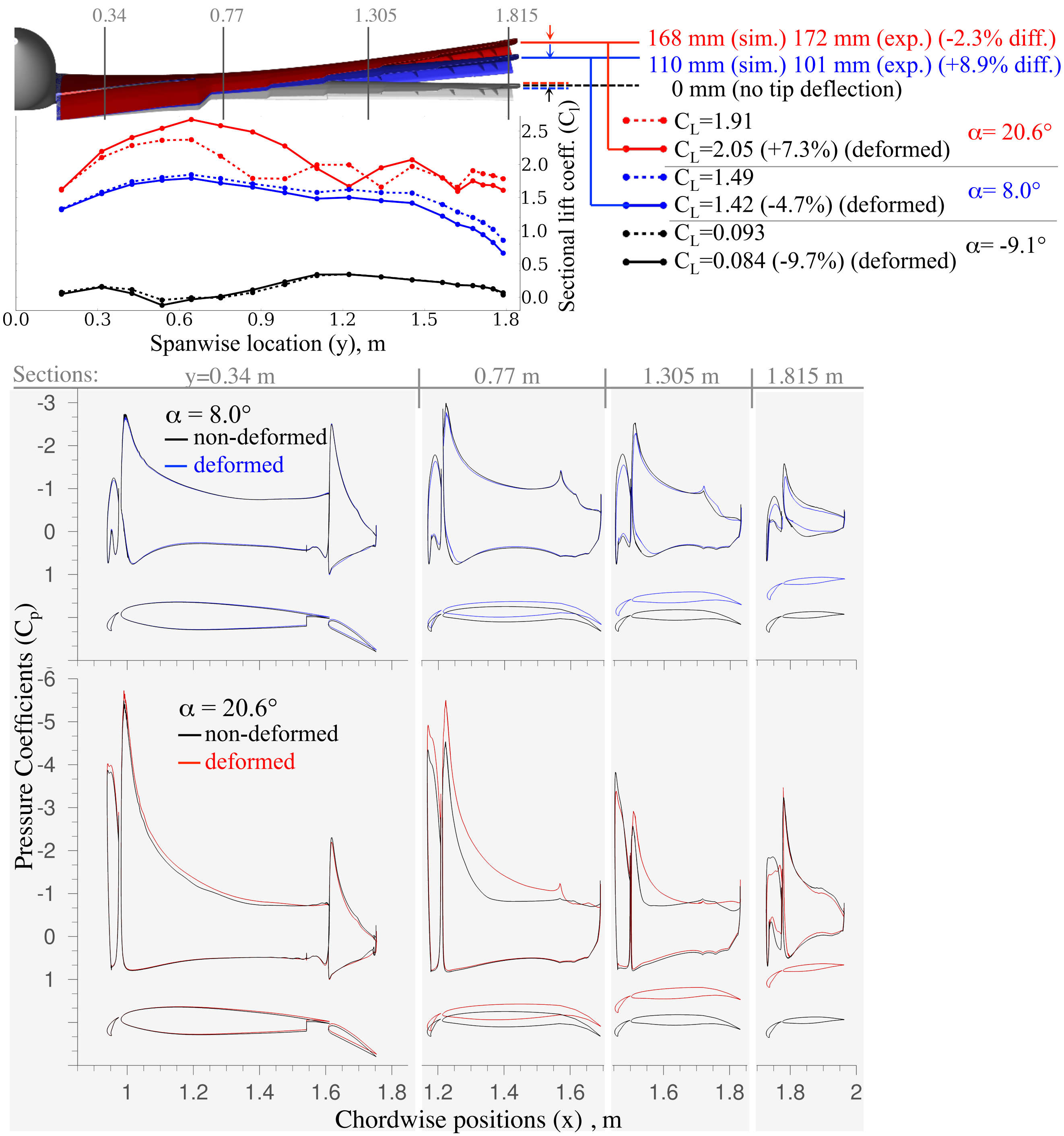

0.34
0.77
1.305
1.815
168 mm (sim.) 172 mm (exp.) (-2.3% diff.)
110 mm (sim.) 101 mm (exp.) (+8.9% diff.)
0 mm (no tip deflection)
C_L=1.91
C_L=2.05 (+7.3%) (deformed)
α= 20.6°
C_L=1.49
C_L=1.42 (-4.7%) (deformed)
α= 8.0°
C_L=0.093
C_L=0.084 (-9.7%) (deformed)
α= -9.1°
Sectional lift coeff. (C_l)
Spanwise location (y), m
Sections:
y=0.34 m
0.77 m
1.305 m
1.815 m
α = 8.0°
non-deformed
deformed
α = 20.6°
non-deformed
deformed
Pressure Coefficients (C_p)
Chordwise positions (x) , m

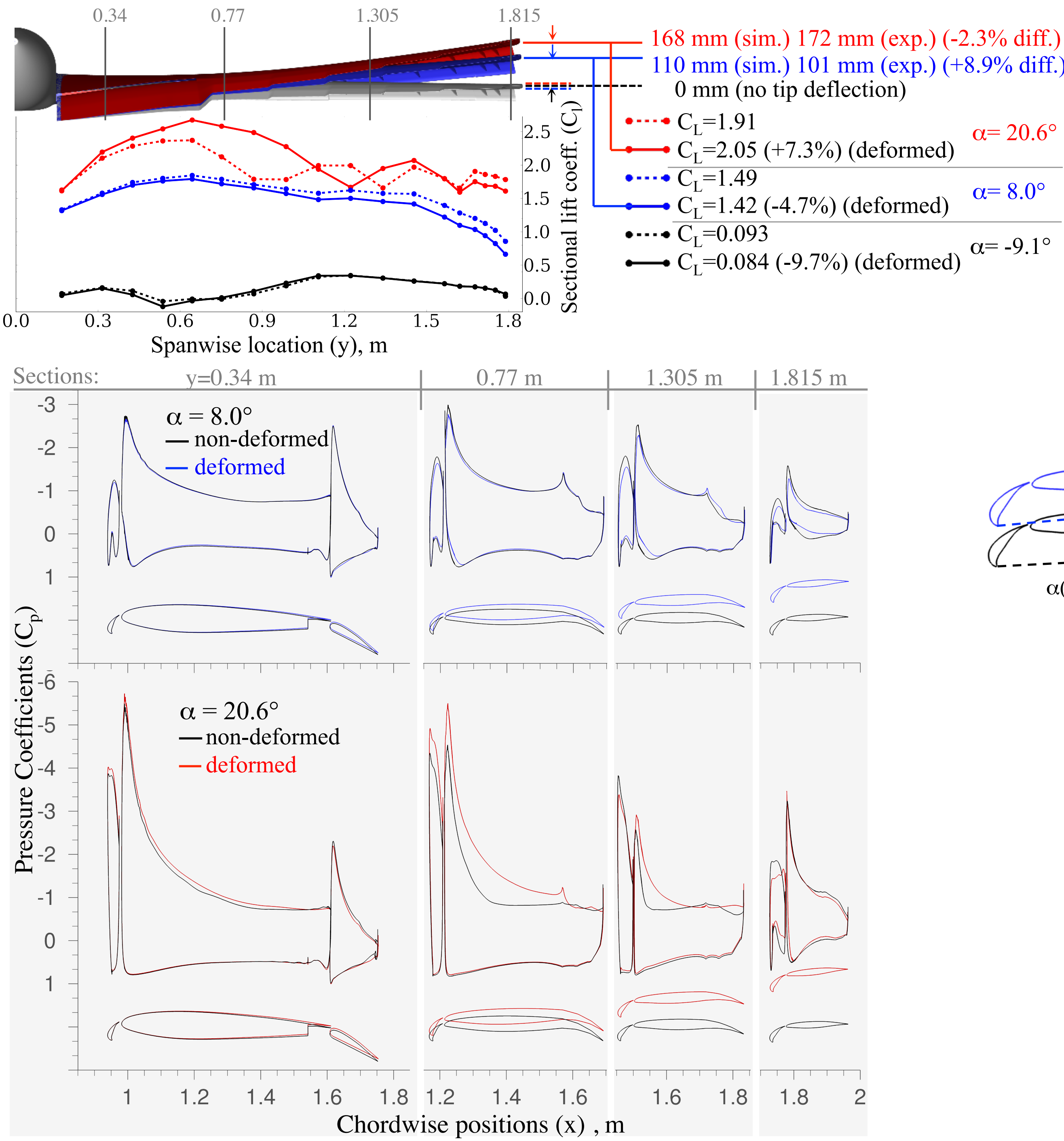

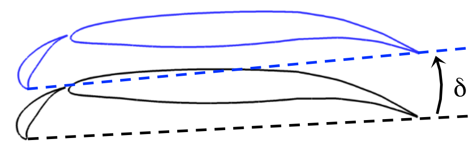

α(y,def.) = α(y,non-def.) – δ(y)

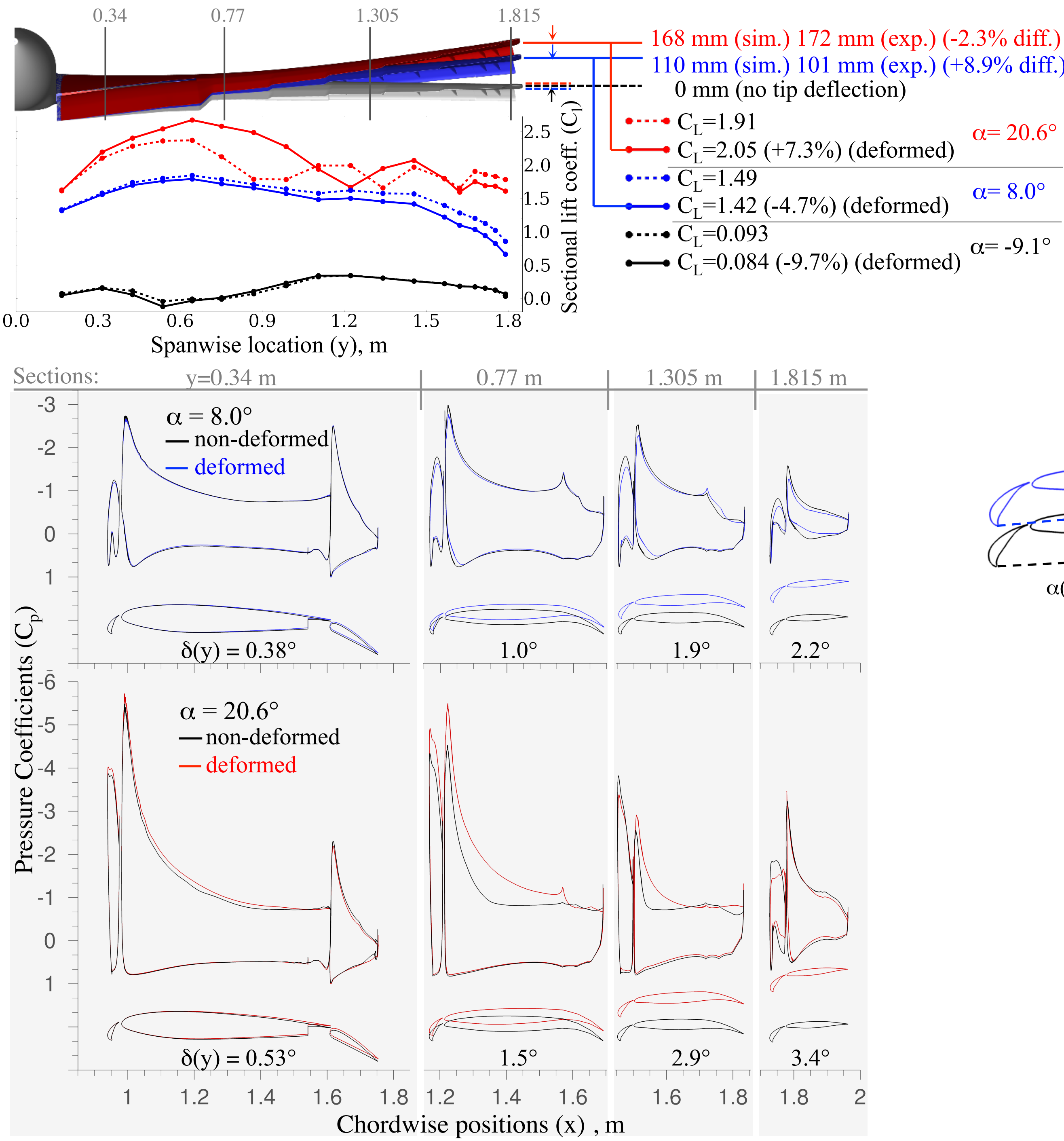

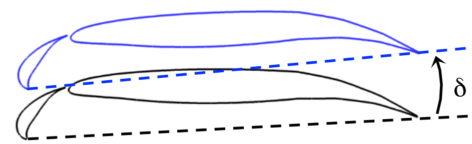

α(y,def.) = α(y,non-def.) – δ(y)

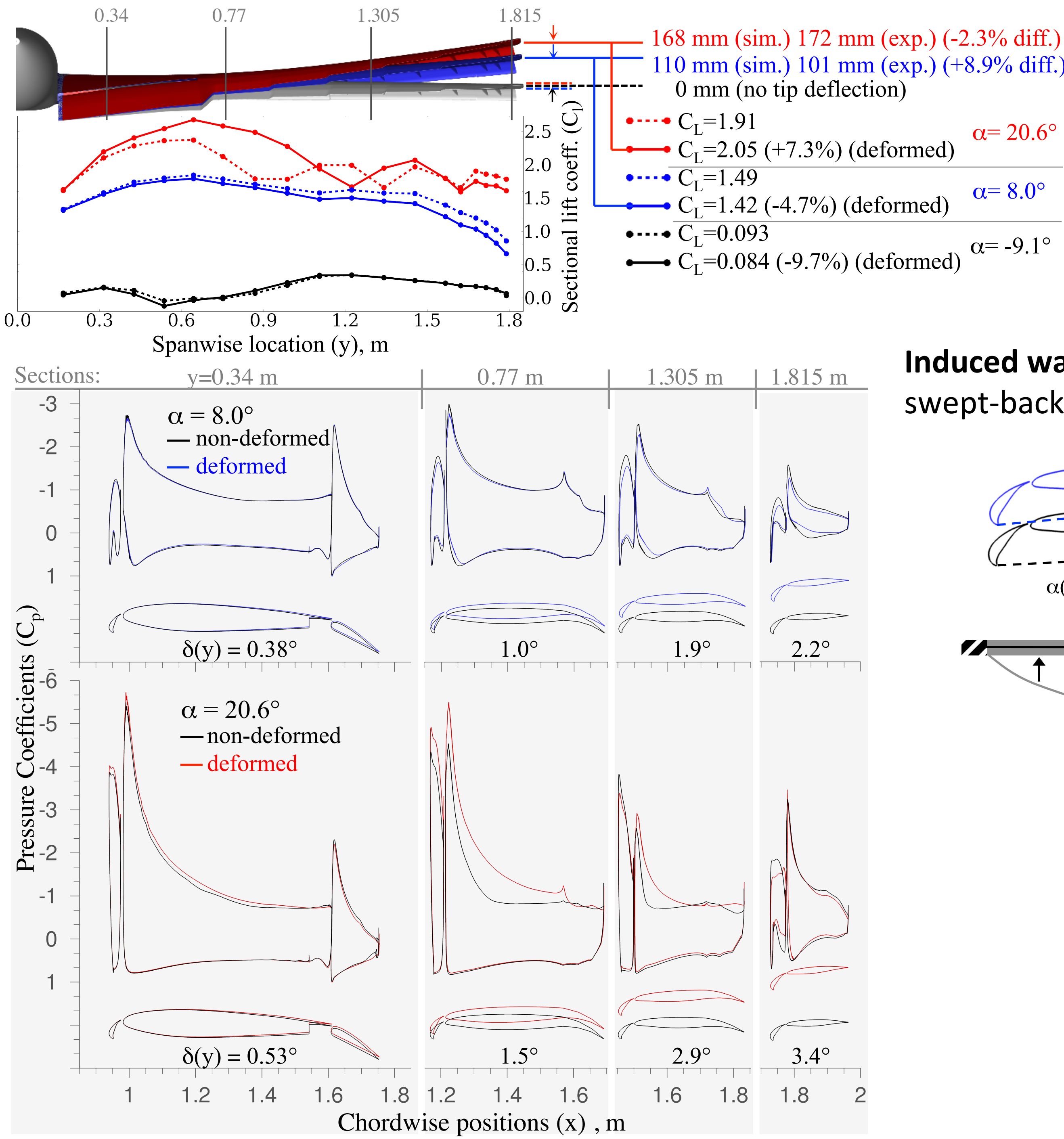

Induced washout: Pitch-down twist of swept-back wings under lift forces.

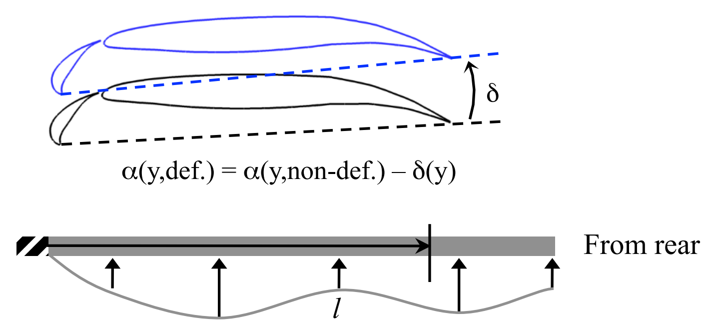

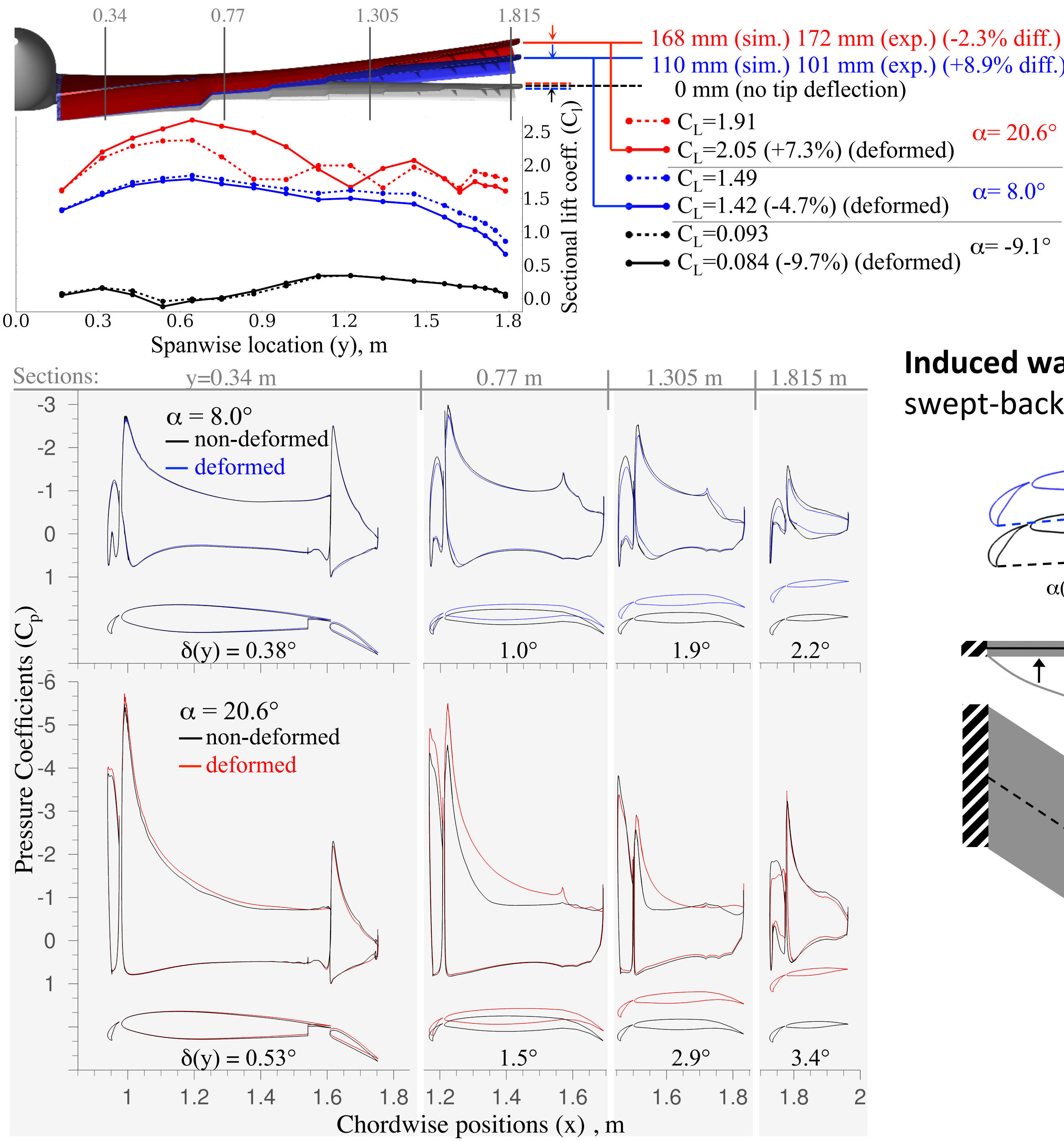

Induced washout: Pitch-down twist of swept-back wings under lift forces.

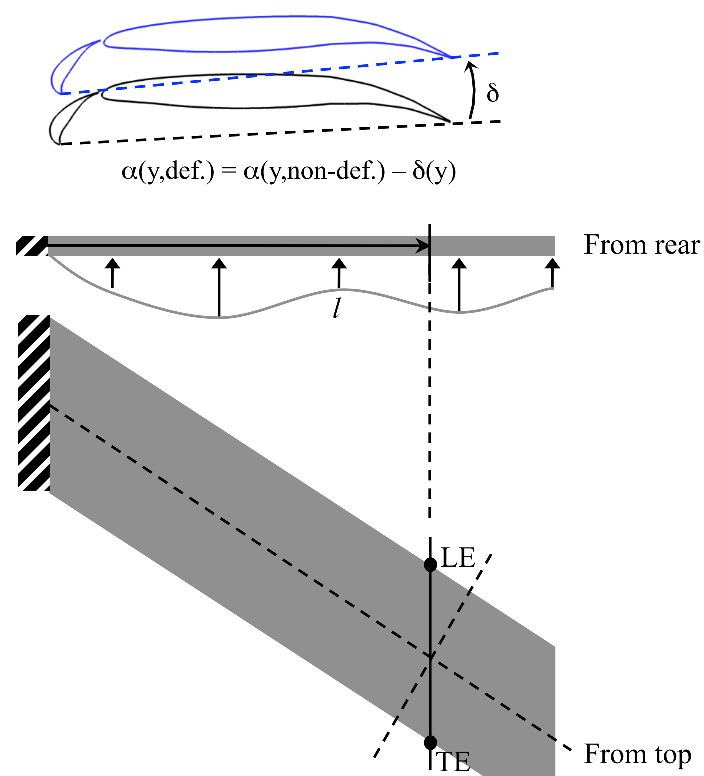

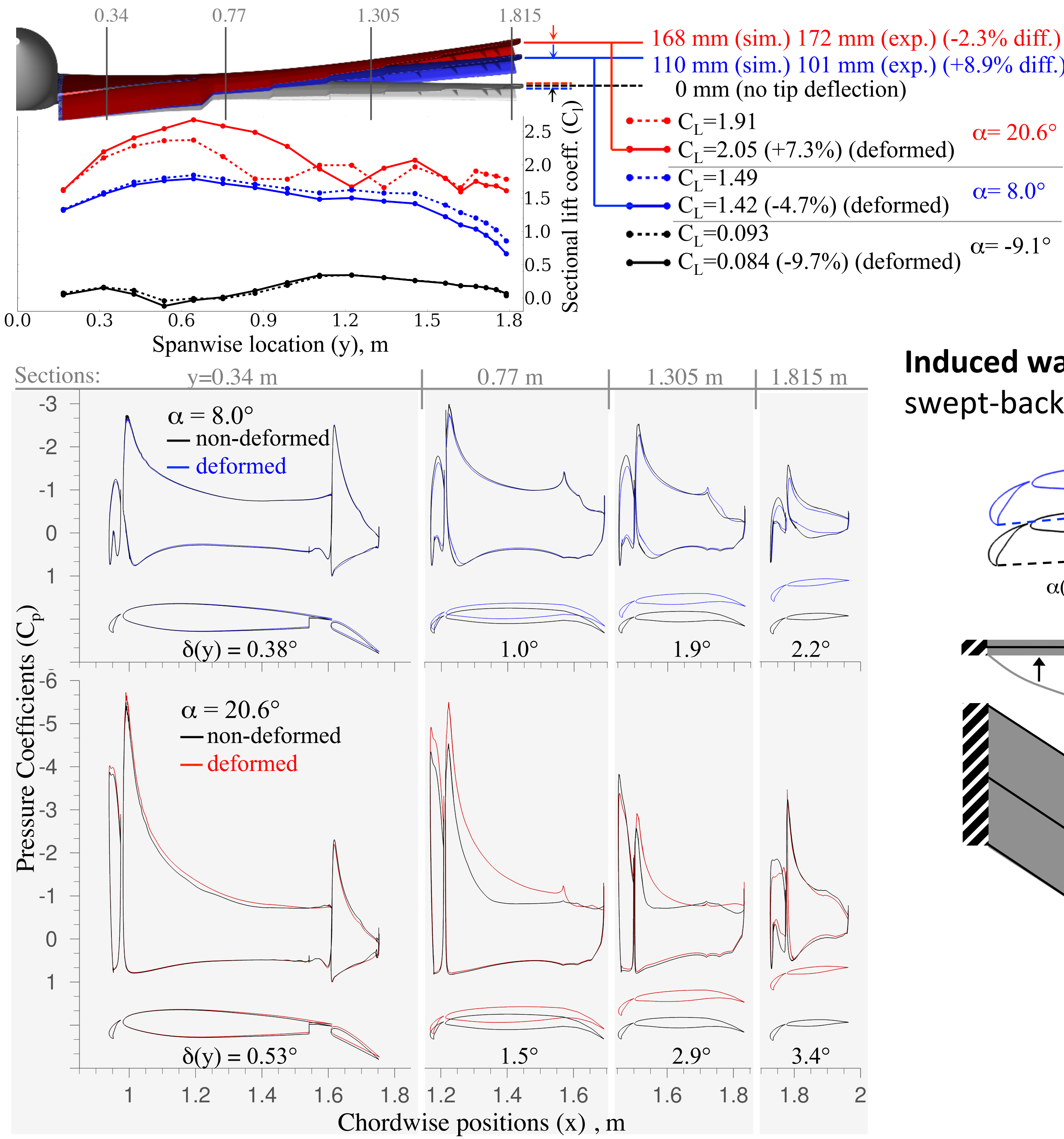

Induced washout: Pitch-down twist of swept-back wings under lift forces.

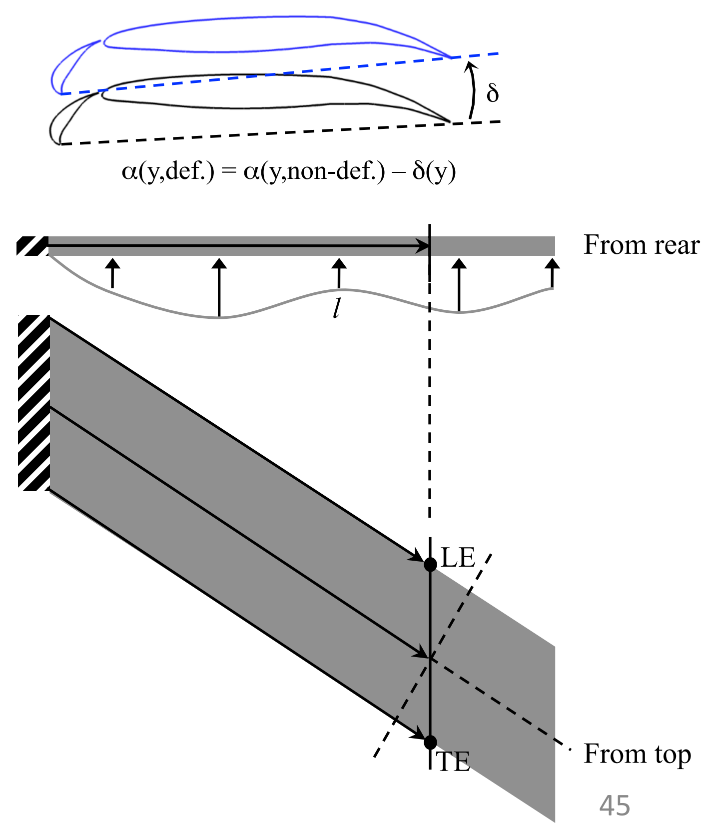

Induced washout correction

The lift coefficients obtained from Overflow simulations with non-deformed wings can be corrected for local changes in angle of attack due to induced washout:

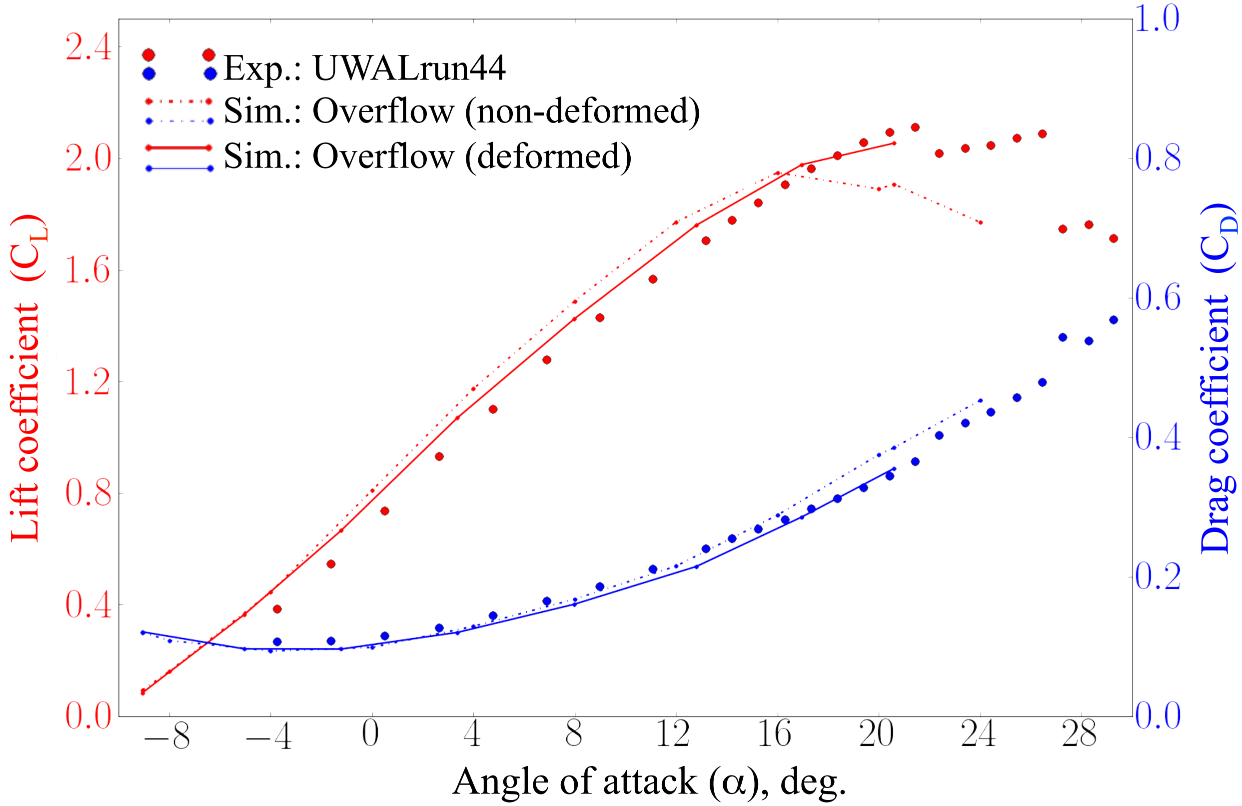

Induced washout correction

The lift coefficients obtained from Overflow simulations with non-deformed wings can be corrected for local changes in angle of attack due to induced washout [5]:

$C_{L,\text{ non-def.}}$ vs α curve for the entire geometry with the non-deformed wing is available.

- Extract $C_{l,\text{ non-def.}}$ vs α curve for multiple sections *s* of the non-deformed wing
- Calculate the amount of induced washout (δ_s) for each section using beam elements method. (Local angle of attack α_s for each section now is as $\alpha_s=\alpha-\delta_s$)
- Using the $C_{l,\text{ non-def.}}$ vs α slopes of the each section, predict the sectional lift coefficients of the deformed wing as

$$C_{l,\text{ def.}} = C_{l,\text{ non-def.}} + \delta_s dC_{l,\text{non-def.}}/d\alpha$$

- Integrate the sectional loads $C_{l,\text{ def.}}$ and add fuselage contribution to find $C_{L,\text{ def.}}$, the lift coefficient of the entire vehicle with deformed wing.

(No need to run Overflow again, just alter Overflow's lift prediction for non-deformed wings)

[5] Nguyen N. *et al*. 2014 *Experimental Investigation of a Flexible Wing with a Variable Camber Continuous Trailing Edge Design* 32nd AIAA Applied Aerodynamic Design Conference at Aviation Forum 2014

Results, revisited

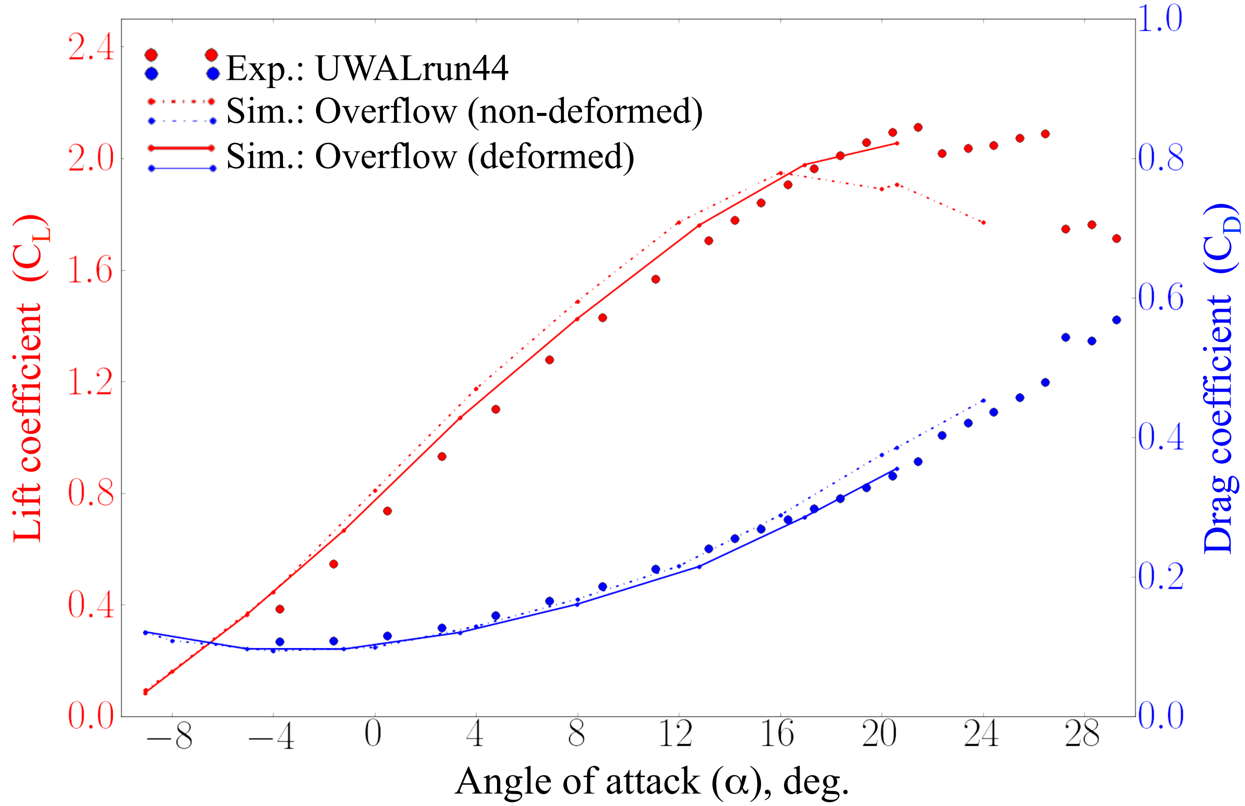

Results, revisited

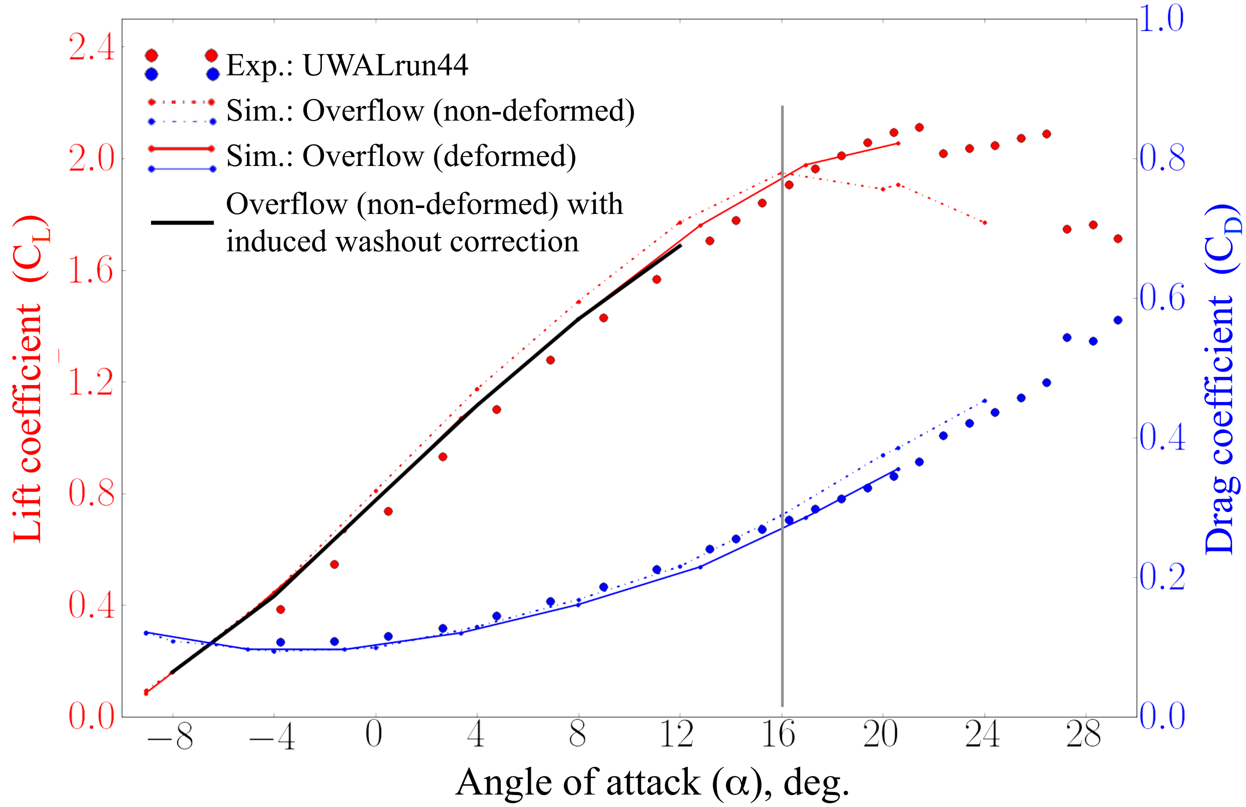

The correction works very well up to α=12°, will probably work until α=16° but fail afterwards due to pervasive separation.

Summary

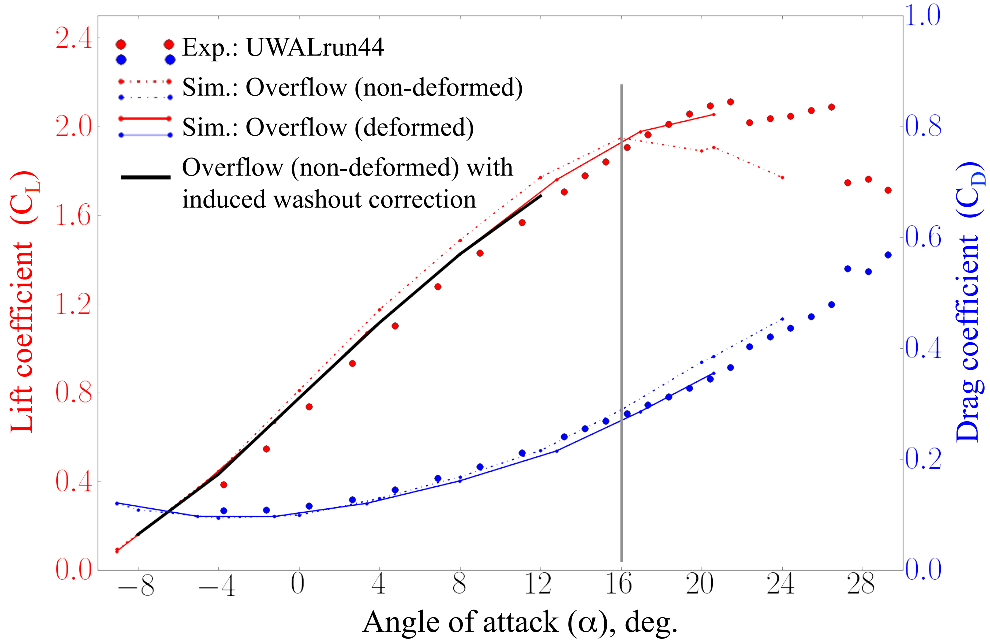

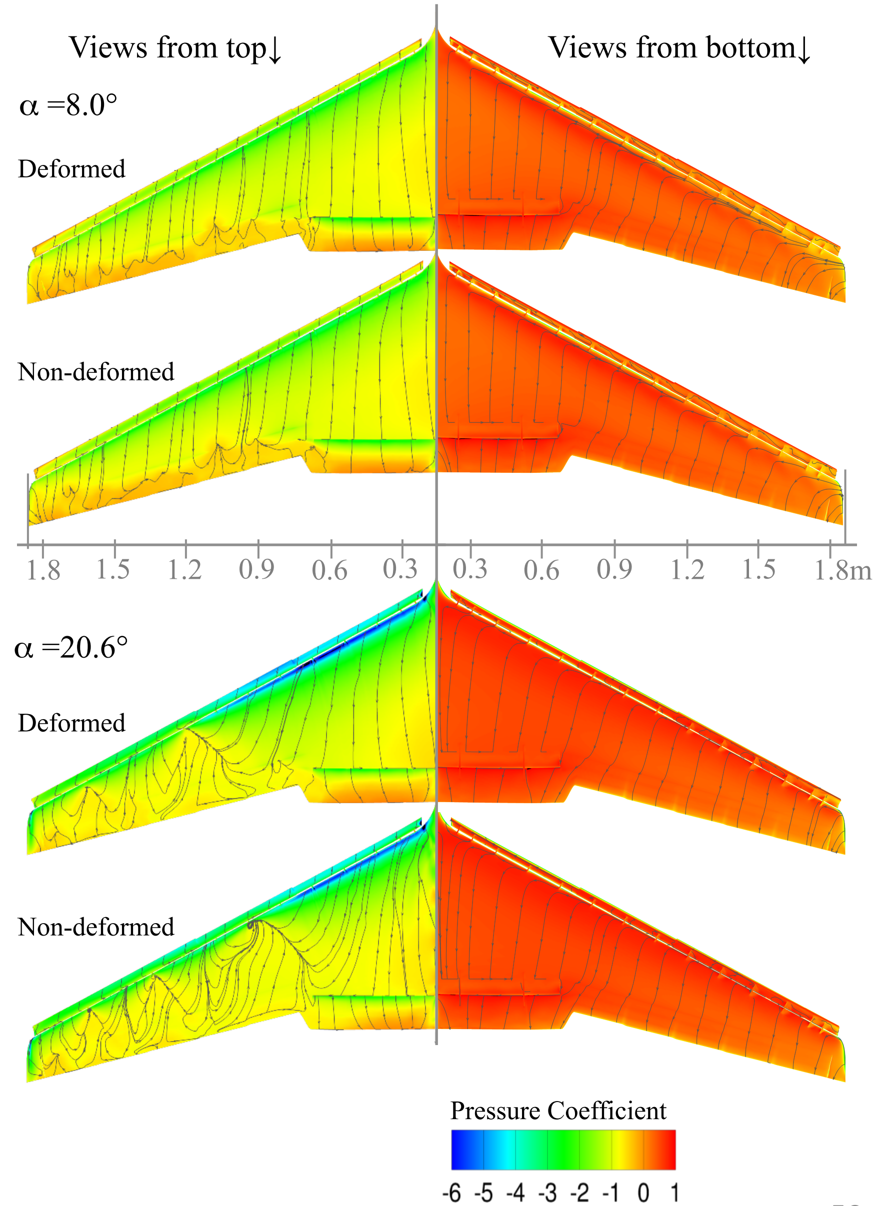

- Induced washout reduces lift at low angles of attack simply by lowering angle of attack further, but increases the lift at higher angles by alleviating stall.

Summary

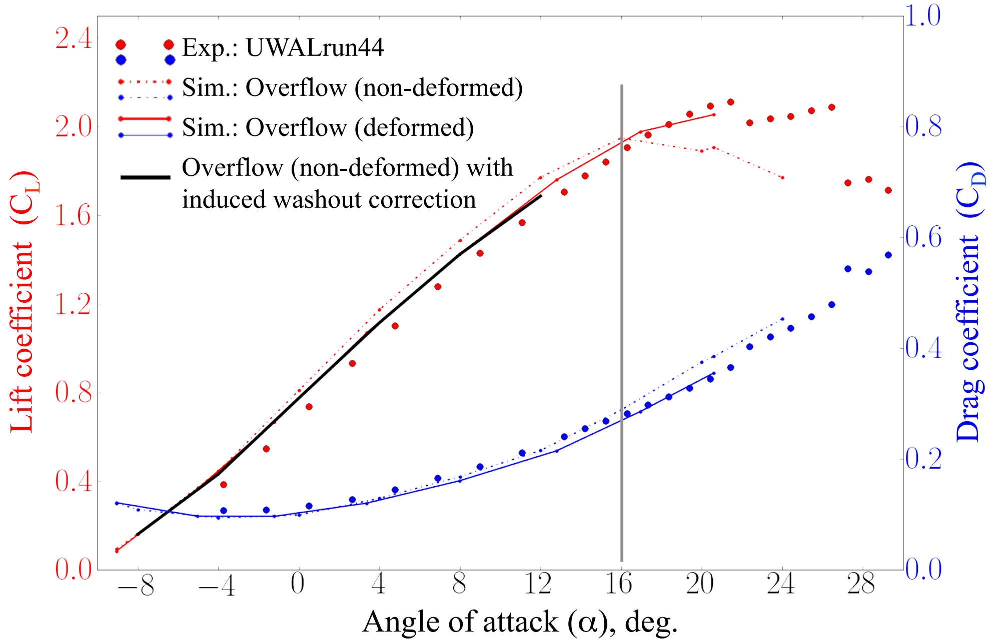

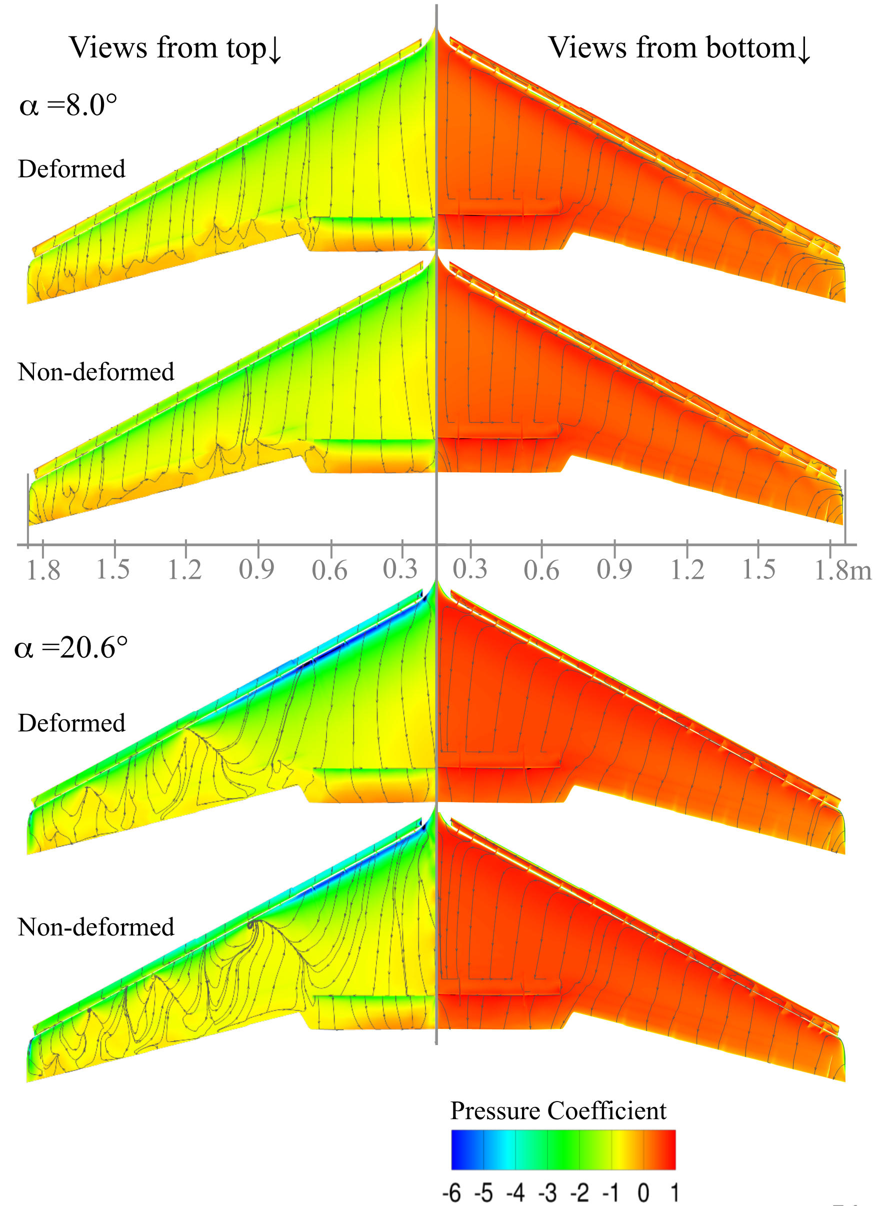

- Induced washout reduces lift at low angles of attack simply by lowering angle of attack further, but increases the lift at higher angles by alleviating stall.

- While the cost of lift predictions can be lowered by corrections at low angles, viscous flow simulations on deformed wings are necessary at high angles.

Summary

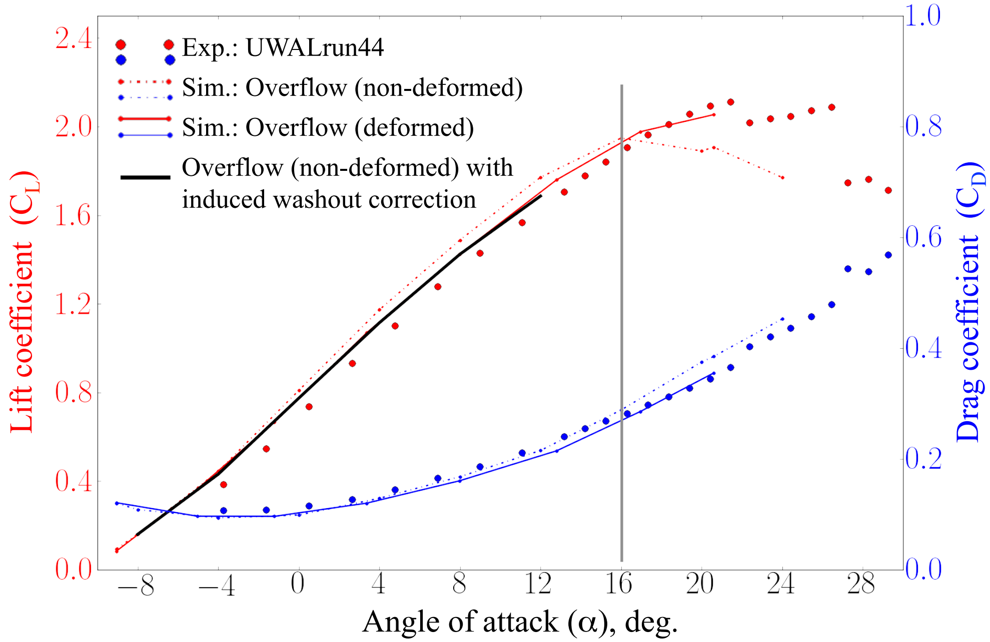

- Induced washout reduces lift at low angles of attack simply by lowering angle of attack further, but increases the lift at higher angles by alleviating stall.

- While the cost of lift predictions can be lowered by corrections at low angles, viscous flow simulations on deformed wings are necessary at high angles.

- In this work, we successfully predicted lift of a flexible wing at high-lift conditions by using both inviscid and viscous flow simulation tools in a cost-effective framework.

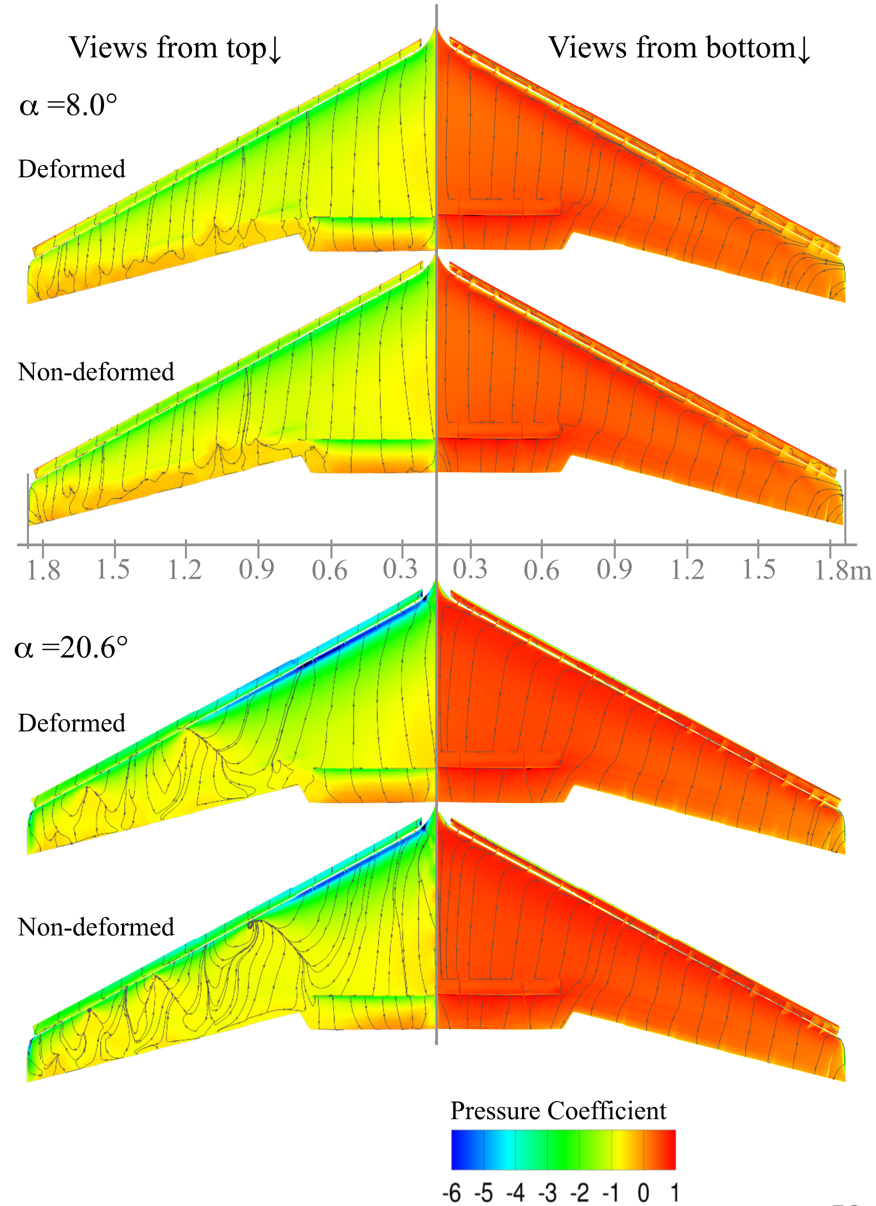

Model Information

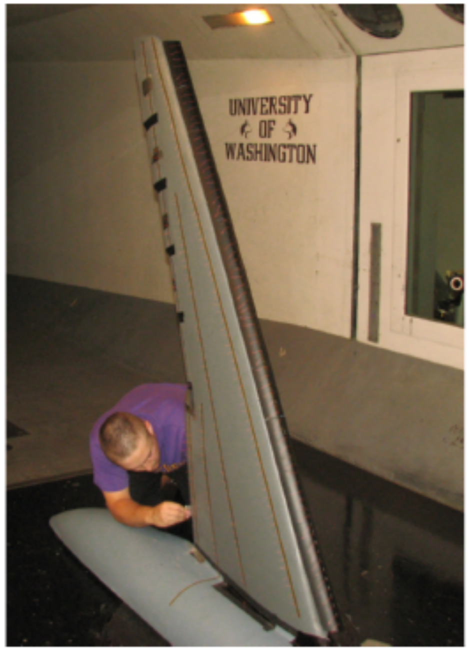

Test conditions:
$q_\infty \approx 282$ Pa
($U_\infty \approx 21.5$ m/s, $M_\infty \approx 0.062$
in air at 101,325 Pa at $T_\infty = 26°$ C)

Wind tunnel tests were conducted at University of Washington Aeronautical Laboratory during the summer of 2014.

The model has a set of slats, an inboard flap and a VCCTEF (Variable Camber Continuous Trailing Edge Flap), all deployed for a high-lift configuration.

Bending and torsional stiffness of the wing is tailored to be representative of modern, composite-wing aircrafts.

Detailed Analysis

Sectional variations:

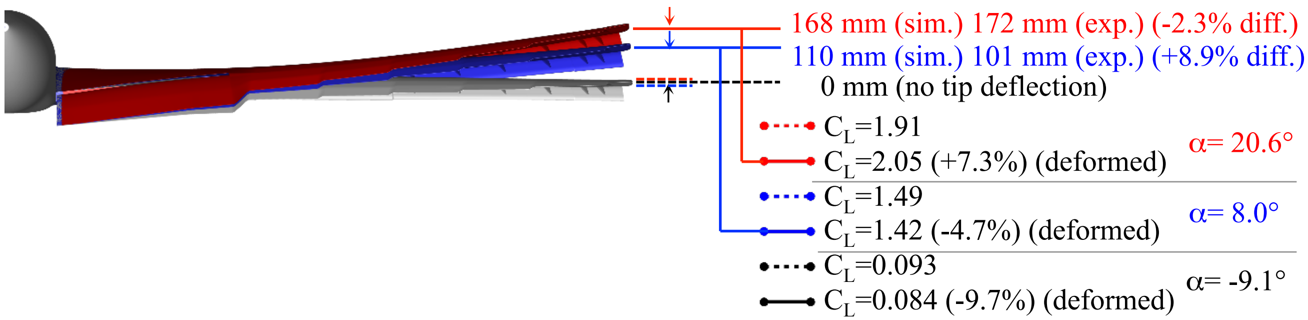

Detailed Analysis

Sectional variations:

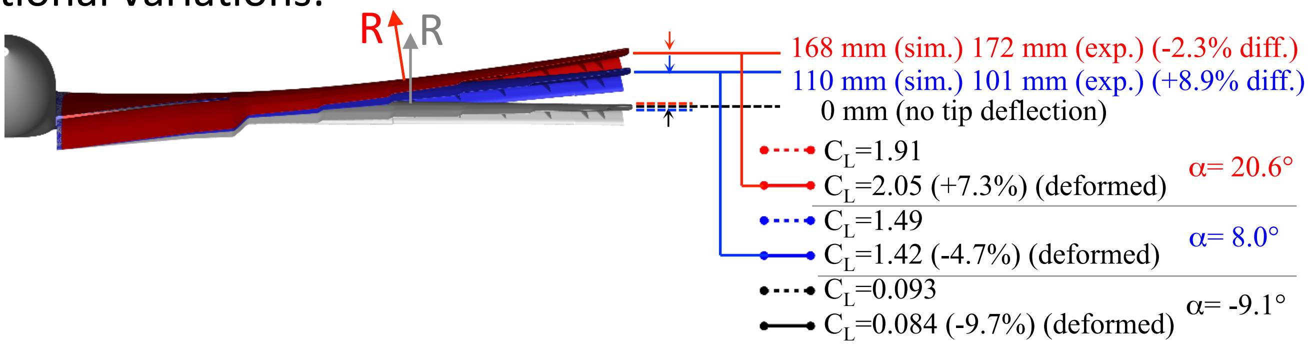

Rotation of lift resultant force due to induced dihedral angle decreases lift by 1% or less, which is minor, and it cannot *increase* lift.